Meta-Analysis of Geomorphodynamics in the Western Lower Bakırçay Plain (Aegean Region, Turkey)

Fabian Becker [1,*] , Daniel Knitter [2] , Moritz Nykamp [1] and Brigitta Schütt [1]

[1] Physical Geography, Department of Earth Sciences, Institute of Geographical Sciences, Freie Universität Berlin, 12043 Berlin, Germany; m.nykamp@fu-berlin.de (M.N.); brigitta.schuett@fu-berlin.de (B.S.)

[2] Physical Geography I: Landscape Ecology and Geoinformatics, Institute of Geography, Faculty of Mathematics and Natural Sciences, Christian-Albrechts-Universität zu Kiel, 24098 Kiel, Germany; knitter@geographie.uni-kiel.de

*   Correspondence: fabian.becker@fu-berlin.de

Abstract: The relation between human activities, climate variability, and geomorphodynamics in the Mediterranean region is widely discussed. For the western lower Bakırçay plain in the ancient Pergamon Micro-Region, geoarchaeological studies have shown changes in geomorphodynamics primarily on a site-basis. We reconstruct past geomorphodynamics in the area based on a meta-analysis of 108 ^{14}C-ages obtained from 25 sediment sequences mainly from colluvial and alluvial deposits by analyzing cumulative probability functions of the ^{14}C-ages. Accounting for biases in the database, we applied different approaches and compared the empirical probability functions with simulated functions. Reconstructed geomorphodynamics in the western lower Bakırçay plain during the Holocene principally coincide with a trend of climate-driven sensitivity to erosion and population dynamics in the eastern Mediterranean, but are also related to the local settlement history. Our data analysis shows that transformations of the Pergamon Micro-Region between the Hellenistic and Roman Imperial times is contemporary to increasing geomorphodynamics that peak in Roman Imperial times. However, a cause–effect relationship between geomorphodynamics and settlement dynamics should be further evaluated. A comparison with data from other settlement centers in Anatolia shows that a coincidence between the peak in geomorphodynamics and a peak in settlement activity are not obvious and may be influenced by soil conservation measures, preferred settlement location, and inherited soil exhaustion.

Keywords: cumulative probability functions; fluvial activity; sedimentation rate; fluvial aggradation; geoarchaeology; alluviation; Asia Minor; Anatolia; Pergamon

1. Introduction

Ever since Claudio Vita-Finzi's seminal book *The Mediterranean valleys: geological changes in historical times* [1], the varying importance of climate and human control on soil erosion by water in the Mediterranean region has been discussed [2–6]. In a review on Holocene environmental change in the eastern Mediterranean, Dusar et al. [7] identified several phases in which sediment dynamics changed. They stress the decreasing importance of climate control over erosion sensitivity during the Holocene and the coincidentally increasing importance of human impact [7]. The authors additionally state that both erosion sensitivity and sediment dynamics mainly increased from the Early Bronze Age to Late Antiquity. In addition to a general trend of changes in the importance of human impact on sediment dynamics in the eastern Mediterranean, local and regional studies offer a nuanced view on the topic [8]. This becomes especially important when considering different types of archives along a sediment cascade [8–12].

Human impact is especially important in the context of a micro-region of large settlements, i.e., settlements where the requirements for e.g., fuel wood and agricultural areas clearly exceeded

the capacity of the landscape in its direct surroundings [13–15]. From Anatolia, lots of evidence for changing sediment dynamics under human impact is available from the ancient city of Sagalassos (Burdur province, Turkey), including modeling approaches [16], detailed sedimentological studies [17–19], and a meta-analysis of sediment dynamics [8]. Similar analyses for Aegean Anatolia are not available at present. Most sedimentological and geoarchaeological studies in the Aegean region focus on coastal locations [20–33].

1.1. Sediment Dynamics in the Western Lower Bakırçay Plain

For Elaia, the "maritime satellite" of the ancient city of Pergamon [34,35] (the modern city of Bergama) (Figure 1), geoarchaeological and sedimentological studies are also available [36–41]. In the bay of Elaia, the construction of breakwaters and moles during antiquity had an impact on local sedimentation rates and styles [39,40]. This change in sediment dynamics was, however, not only due to the constructions of maritime structures and therefore a change in the local depositional environment, but also due to human impact in the contributing catchments [39]. The increasing presence of *Glomus*-type fungi in the sediments from the harbor around 2.7 ka BP, along with an increasing sedimentation rate, indicators of torrential floods, and palynological proxies, point to increased land clearing and subsequent erosion inland after 2.3 ka BP [37,41]. This impact was much more pronounced in the vicinity of the major settlement around the bay compared to more distal locations [37]. The occurrence of torrential floods and consequent siltation presumably resulted in the abandonment of several coastal settlements and made the harbor inaccessible for certain types of ships whose draught exceeded water depth [38,39]. In addition, the development of the Madra delta plain in the direct vicinity of the western lower Bakırçay plain is studied from a sedimentological and geoarchaeological point of view [42–44]. Due to the relatively low chronological resolution, these studies do not give hint to changing geomorphodynamics. However, the studies clearly show the coastal development and the palaeogeography of the area. Coastal dynamics had an influence on settlement conditions; a change from progradation to aggradation in the surroundings of the a settlement hill in the delta area is observed.
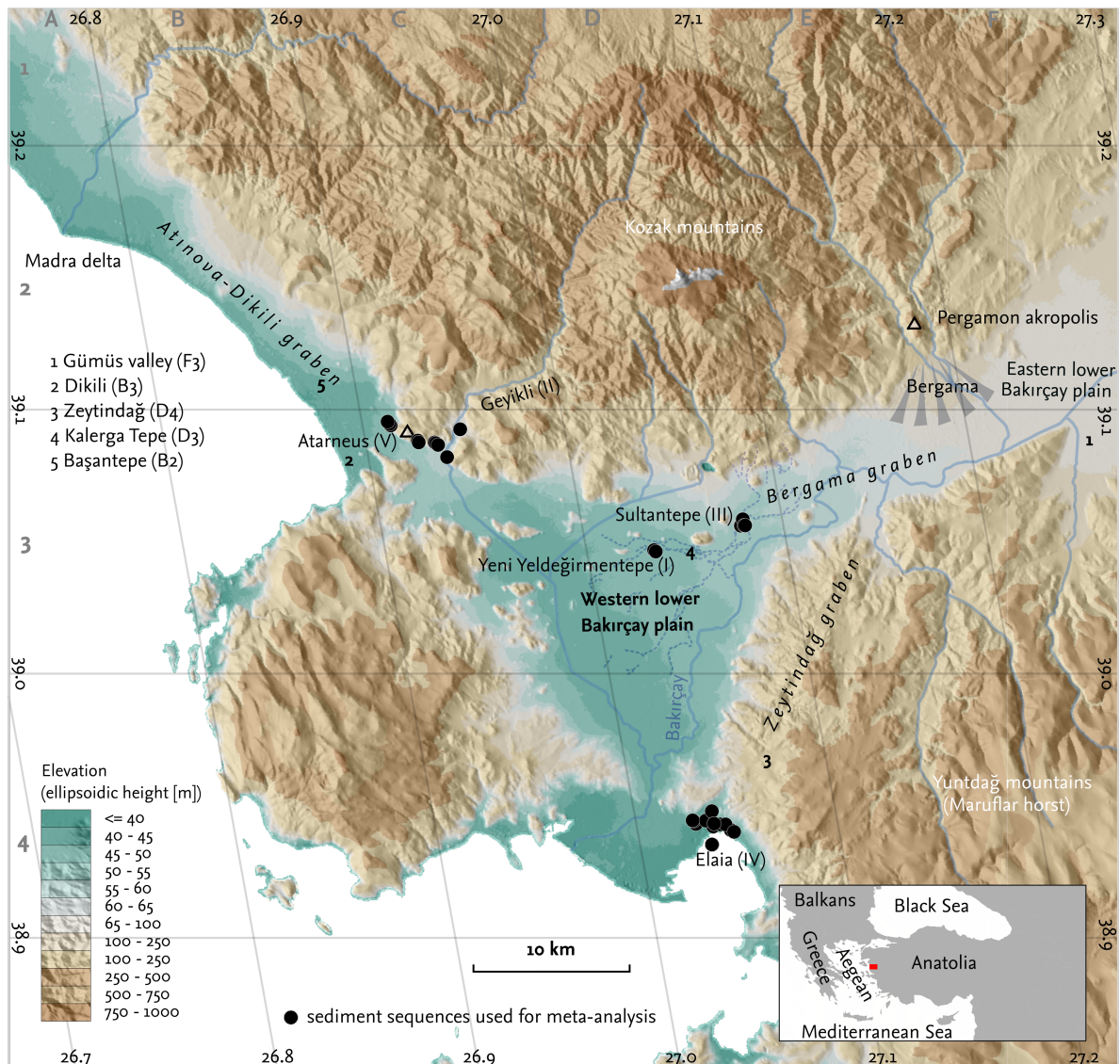
Figure 1. Overview map of the western lower Bakırçay plain. Sampling locations of the sediment sequences referred to in the current study are highlighted; main grabens are named and selected rivers/creeks and settlements are shown (some are indicated by bold numbers). For details on the sediment sequences see Table 1. Database: TanDEM-X digital elevation model [45,46], rivers partly digitized from Open Street Map-data [47]; locations of sediments according to original publications [37–41,48–51].

Studies from the western lower Bakırçay plain revealed changed sediment dynamics in the context of historical settlements [37,49,50]: Fan development originating from the slopes around the acropolis of Atarneus started in the Bronze Age, around 3.1 ka BP. Colluvial sediments in the area date to the Middle–Late Iron Age (ca. 2.7 to 2.4 ka BP.) [49]. Despite a clear change in human activities around Atarneus in the last 3 ka, sedimentation processes did not change much. Schneider et al. [49] attribute this to the construction of terraces on the slopes around Atarneus that reduced soil erosion rates even under intensified land use. In the surrounding of the Late Chalcolithic–Early Bronze Age settlement at Yeni Yeldeğirmentepe, fluvial sediments are intercalated by sediments showing a clear anthropogenic imprint (archaeological remains were uncovered from the respective layers); a change in sedimentation rate coincides with early activities at the site (Figure 3 in [50]). In contrast, there is no change in sediment dynamics related to pre-modern human impact recorded for the Geyikli valley and the environs of the archaeological site near Sultantepe [48,51].

1.2. Objectives and Outline

In addition to the study from the Geyikli valley that did not recover any traces of human impact on sediment dynamics [48], all cited studies from the western lower Bakırçay plain are directly related to human settlements of a specific period, such as the Graeco–Roman harbor at Elaia [39,41] or the Chalcolithic–Bronze Age settlement at Yeni Yeldeğirmentepe [50]. A meta-analysis synthesizing the detailed analyses for the western lower Bakırçay plain is not yet available. Therefore, the main objective of the current study is to re-evaluate the existing sedimentological and geochronological data to reconstruct the general trend in sediment dynamics in the western lower Bakırçay plain.

Our meta-analysis is based on cumulative probability functions (CPFs) of radiocarbon ages sampled from sediment sequences obtained from the western lower Bakırçay plain and its intermediate vicinity. We compare the CPF of the observed ages with a null model of the cumulative probability that can be expected from the ages randomly distributed over the available sediment sequences. The approach is derived from archaeological demography studies [52,53]. Along with an estimation of sedimentation rates and a Bayesian chronological model of facies change, we use the null model approach to reduce the impacts of depositional and sampling biases on the identification of phases of increased geomorphodynamics (see Section 2.3.2).

The generic term *geomorphodynamics* is used in the current study for two reasons. First, the term includes various surface processes—different processes of erosion, deposition, and reworking are covered. With our approach, we analyze the sediments related to these processes. Since different processes, e.g., increased erosivity or reduced vegetation cover due to human impact, can result in the same sedimentary signal, a term covering various processes is most appropriate. This is especially important as climate and human triggers are entangled [54] and one trigger can level or accelerate another one [4,55]. The triggers of changed geomorphodynamics are assessed by comparing the identified phases of increased geomorphodynamics with different proxies of climatic variability, vegetation development, and population dynamics from Anatolia, southern Greece, and the Balkans. Second, the term geomorphodynamics is used if a change in the sediment sequences is indicated by different proxies, i.e., either combination of the following three: a change in the cumulative probability of ^{14}C-ages, a change in the sedimentation rate, or a facies change.

2. Materials and Methods

2.1. Study Area: The Western Lower Bakırçay Plain

The western lower Bakırçay plain is the lowest of the three major plains of the river Bakırçay and lies south-southwest of the Bergama fan (Figure 1). For practical reasons, we included the coastal areas close to Dikili and Zeytindağ to the western lower Bakırçay plain, although this is topographically not consistent. The Bakırçay rises in the Ömer Dağı, flows mainly in east-southeastern direction and drains a catchment area of circa 3350 km^2 into the Aegean Sea [56,57]. The western lower Bakırçay plain covers an area of around 140 km^2.

The climate in the region is a typical Mediterranean hot and dry summer climate of the temperate regions (following the Köppen–Geiger classification [58,59]). Annual rainfall averages 636 mm (Dikili) or 711 mm (Bergama) with a maximum monthly average in December (115 mm, Dikili) and a minimum monthly average in July (<10 mm). The annual average temperature is around 16 °C [60].

The development of the western lower Bakırçay plain is mainly driven by the formation of a horst and graben structure during the Middle Miocene to Early Pliocene (Bergama, Zeytindağ, and Altınova-Lesvos grabens and the Kozak and Maruflar horsts) [61]. Bedrock consists of mainly volcanics (pyroclastic and andesitic rocks in the north and east), intrusive rocks (granodiorite in the headwaters of the north), and carbonate and continental clastic rocks (in the south) [62]. During the Pleistocene, pediments and relatively large fans (such as the Bergama fan) developed on the southern margin of the Kozak horst. Pediments are mainly located in the northern part of the western lower Bakırçay plain due to the asymmetric shape of the horst-and-graben structure; average slope and

size of the catchments of creeks draining the Kozak mountains to the northern part of the western lower Bakırçay plain are greater compared to the catchments of creeks draining the Yunt Dağı mountains in the southern and eastern part of the plain [60,61]. Several andesitic hills (Turkish *tepe*, e.g., Sultantepe and Kalerga Tepe) occur on the northern edge of the western lower Bakırçay plain (Figure 1). A detailed geomorphological characterization of the entire Bakırçay catchment and the Madra catchment, including the adjacent coastal areas, is given in the contribution of Yang et al. in the current special issue [60].

2.2. Database

We collected $n = 108$ ^{14}C-ages from $s = 25$ sediment sequences obtained from the western lower Bakırçay plain and the surrounding areas (Figure 1). The sampling locations comprise alluvial terraces of the Geyikli drainage basin in the north-western part of the western lower Bakırçay plain; the foot slopes of the small volcanic Yeni Yeldeğirmintepe; the transition zone between the piedmont of the Kozak horst and the plain in the northern part of the western lower Bakırçay plain; and the northern part of the Bay of Elaia, where sediments mainly originate from the slopes and small drainage basins of the Yunt Dağı mountains (Table 1). The archives at these different sample locations react differently on disturbances such as land-use change or changing precipitation. Deposits from low order catchments resulting in, e.g., colluvial layers, are directly related to local human impacts if there is e.g., a settlement in the close vicinity [10,11]. Sediment archives from high order catchments, e.g., the Bakırçy floodplain, by contrast, react less directly to local human impact—their signal rather gives an average of changes within the wider catchment area. Compared to colluvial deposits, floodplain deposits of larger catchments are thus less sensitive to local human impact of the same scale, but can react equally sensitive to changes in precipitation. In addition, the residence time of the deposits within these archives differs considerably [63].

For all available ^{14}C-ages (see Figure 2), metadata were collected from the original publications, i.e., sampling depth, total depth of the sequence, uncalibrated ^{14}C-ages, lab errors, and information on a potential reservoir effect. Additionally, the lithostratigraphy and physical/chemical data of the sediment as given in the original publication were used to categorize the data into change classes [64–67] (Figure 2). Ages were classified as "change-before ages" if a major change in sediment facies is indicated in ≤25 cm below the sampling depth ($n = 37$) and as "change-after ages" if a facies change is indicated in ≤25 cm above the sampling depth ($n = 23$). Ages were classified as "no-change ages" if they are stratigraphically not related to changes in sediment facies ($n = 27$). For $n = 21$ ages, no information on a facies change is available. For all sediment sequences with available ^{14}C-ages, we also collected lithostratigraphic information from the original publications. As a result that the terms used to describe the lithostratigraphic units differ between the publications, we harmonized the data. The ^{14}C-ages were on a first level categorized as ages from terrestrial or marine sedimentary units (Figure 2).
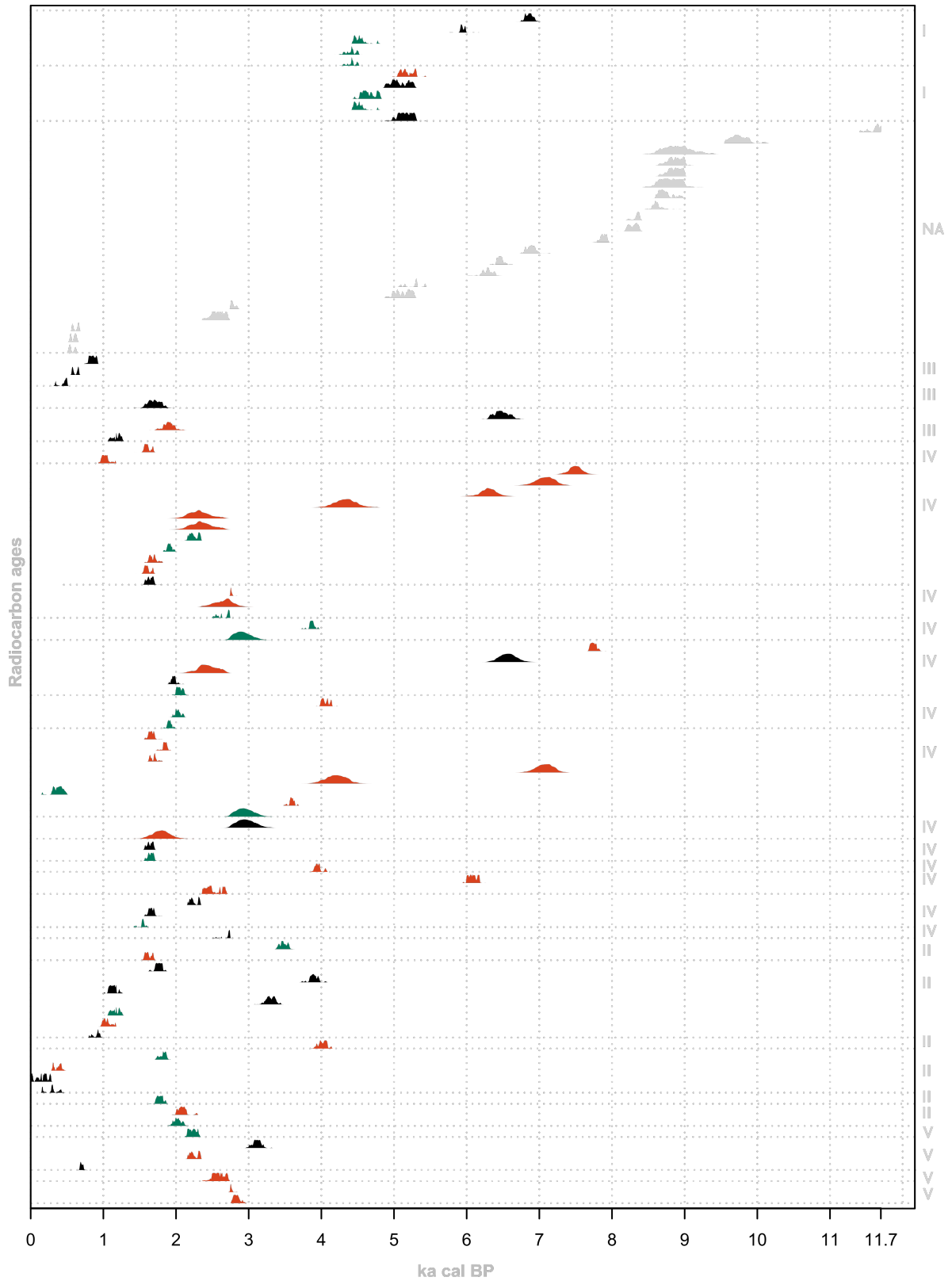
Figure 2. Overview on all ^{14}C-ages from the western lower Bakırçay plain included in our data base. Colors indicate different change-ages (black = no change, green = change-before, red = change-after) and ages where no stratigraphic information are available (grey). Horizontal dashed lines separate different sediment sequences. Probabilities of the dates are not normalized to sum to unity. Secondary y-axis: Location codes as given in Table 1 and Figure 1. Ages obtained from [37–41,48–51].

Table 1. Overview of the sediment sequences included in our meta-analysis. More details can be found in the Supplementary Materials and the original publications. The locations are shown in Figure 1. For $n = 21$ samples, no detailed information on sediment sequences and geomorphological setting is available. s = number of sediment sequences from location; n = number of ^{14}C-ages from location.

Location	Sediment Sequences	Geomorphological Description
(I) Yeni Yeldeğirmentepe	^{14}C-ages mostly from *fluvial* sediment layers, some from *cultural layers* [50]; $s = 2$; $n = 10$	Northern part of the western lower Bakırçay plain, transition zone of the footslope of a small andesitic hill (circa 70×100 m) and the wide alluvial flat of the Bakircay plain; 1st order catchments (<0.001 km^2)
(II) Geyikli valley	Fan/colluvial/sheetflow layers, overbank sediments, braided channel and bar sediments; ^{14}C-ages mainly from fan and sheetflow deposits [48]; $s = 3$; $n = 7$	Outcrops at the bank/terrace edge of the Geyikli creek, the catchments covers circa 95 km^2, the lower Geyikli course is characterised by a narrow valley, fluvial terraces, and the streambed [48]
(III) Sultantepe	^{14}C-ages mainly from channel-related layers, one from overbank sediments [51]; $s = 4$; $n = 8$	Slightly elevated position in the floodplain of the river Bakırçay, close to the border of the piedmont of the Kozak mountain; sediments affected by the Bakırçay (catchment > 2000 km^2).
(IV) Elaia	Dating material from marine and terrestrial layers, the latter comprising fluvial and colluvial sediments [37–41]; $s = 14$; $n = 34$	Closed and open harbor, open bay (sediments classified as marine) and low-order catchments of the littoral plain [37] (catchment area < 3 km^2; area lies east of the Bakırçay delta)
(V) Atarneus	Dating material obtained mainly from fan and overbank sediments [49]; $s = 8$; $n = 17$	Transition zone between footslope of a promontory of the Kozak mountains and the adjacent sedimentary plain (alluvial fans) [49]; 1st and 2nd order catchments (<0.5 km^2)

2.3. Chronological Modeling

All statistics were computed in R version 3.6.2 (2019-12-12) [68]. Packages used for data processing and visualization include *plotrix* [69], *rcarbon* [70], *RColorBrewer* [71], *rioja* [72], *tidyverse* [73], and *zoo* [74].

Maps were created in QGIS Version 3.4.11-Madeira (2019-08-16) [75]; maps and figures were post-processed in Inkscape Version 0.92.4 (14 January 2019) [76]. A detailed description of the computational procedure can be found in the Supplementary Materials.

2.3.1. Calibration and Observed Cumulative Probability Function (CPF)

All ^{14}C-ages were calibrated in R using the *rcarbon* package. The used calibration curves are IntCal13 for terrestrial ages and Marine13 for marine ages that are affected by a reservoir effect [77]. Following Crema and Bevan [53] (see [78]), we did not normalize the age probability distributions of the calibrated ages to unity to avoid artificial peaks in the observed CPF (Figure 3a). The observed cumulative probability function is calculated by summing the dating likelihood of all non-normalized calibrated ^{14}C-ages for all ages dating between 0 BP and 11,700 BP (so covering the Holocene Epoch). The formal subdivision of the Holocene is based on Walker et al. [79]: Boundary between Pleistocene and Holocene at 11.7 ka BP; between Early and Middle Holocene at 8.2 ka BP; and between Middle and Late Holocene at 4.2 ka BP.

The main principle behind the calculation of CPFs from sediment archives is the assumption that an increase of the CPF is proportional to increased deposition when using data from several sediment sequences (e.g., [80]); the record of a single sequence is believed to be fragmented [81,82].

2.3.2. Biases Affecting Cumulative Probability Functions

The application of cumulative probability functions (CPFs) for sedimentological analysis ignited debate (e.g., [80,83,84]; see also [85]). The main critique of the application of CPFs to reconstruct sediment dynamics and especially fluvial activity arises from the nature of depositional and taphonomic processes and the sampling of the dating material. Several biases hamper a straightforward relationship between CPFs and sediment dynamics.

One issue is the effect of the shape of the calibration curve on a CPF; steeper parts of the curve cause peaks in the CPF [86]. Furthermore, the formation of dating material (especially charcoal and plant remains) is not necessarily contemporaneous to transport or final deposition of the material and, thus, the processes related to sediment dynamics [80]. Additionally, in sedimentary archives, dating material and the sediment layers containing the samples are susceptible to erosion and reworking. Thus, preservation cannot be premised [80,82,85,87,88]. The preservation potential of dating material and the sediment layer containing the dating materials decreases with increasing time difference to the moment of sampling (similar to the Sadler-effect [89]; see, e.g., [90,91]).

A 'researcher' bias may cause further problems. For instance, in geoarchaeological studies focusing on a specific period, researchers may try to well capture this period with their geochronological framework [92,93]. Furthermore, the uncovered depth of a sediment sequence may lead to an additionally increased likelihood that younger samples are selected; the thickness of the sediments may be larger than the sampling depth. The availability of dating material is further affected by a 'production' bias: Human-induced (wild) fires in a specific period may increase the likelihood that dating material from this period is sampled, although sediment dynamics may not have changed [85]. Sample size is crucial when dealing with biases in the record of ^{14}C-ages [94]. In small data sets, single ages have a greater impact on the shape of the curve of a CPF.

To cope with potential biases in our data set, we estimated a 'null model' of simulated CPFs and compared them with the observed CPF to test for the reliability of the periods of increased sediment dynamics in our data set from the western lower Bakırçay plain. Additionally, we did a CPF-based estimation of sedimentation rates [8].

2.3.3. A Null Model

A common approach in archaeological demography to reduce the effect of biases is to compare the empirical data from ^{14}C-ages with a null model, i.e., a hypothesis of the shape of the CPF [52,92,95–97]. Our null model is based on the expected likelihood that a point in time is covered with the given sediment sequences. Therefore, we estimated the period covered by each sediment sequence. The underlying hypothesis is that the change in the cumulative probability increases with time, e.g., due to the higher probability that a piece of dating material is preserved, uncovered, and sampled. The minimum age of a sediment sequence s is set to 0 BP; the maximum age is estimated as a function of the total thickness of the sediment sequence and the average sedimentation rate given by the depth and the median age of the calibrated ^{14}C-ages of the sediment sequences. Sequences for which only one ^{14}C-age is available, the maximum age of the sequence is estimated by dividing the thickness of the sequence by the sedimentation rate of the given ^{14}C-age (Appendix A.2).

If more than one sample is available for a sequence, the maximum age of the sequence is estimated based on a power regression age–depth model. Although residuals of the model may be high, this approach is appropriate for the estimation of the maximum age and to account for the preservation bias of the sediment record. Other approaches, such as the estimation of the mean sedimentation rate of a sediment sequence [8,86], are less sensitive to changes in sedimentation rate with increasing range between sampling and recorded age (the so-called 'Sadler effect' [89], see [8]).

In total, 1000 CPFs were simulated. For each of the simulated CPFs, several calendar years were randomly sampled from the period between 0 BP and 11,700 BP. The likelihood that a year in that period is sampled is equal to the proportion of all available sediment sequences covering the respective year. The number of samples taken for each simulated CPF is equal to the number of available ^{14}C-ages

from the study area. With this approach, the sampling density in the original data set is taken into account. For the simulation of a CPF, the random calendar ages where back-calibrated to raw ^{14}C-ages and again calibrated (the estimated error is 40 years for all ages regardless the age of the sample). This approach is necessary to ensure that the observed and simulated CPF both have the same shape for same ages.

The variability in the simulated CPFs is considered by calculating confidence intervals of the simulated CPFs. We furthermore subtracted separately each simulated CPF from the observed CPF. The likelihood that the observed CPF is not increased in a year due to variation in the calibration curve or a sampling bias is equal to the proportion of simulation runs in which the observed CPF is higher than a simulated CPF (the null model). We also normalized the observed CPF by dividing through the cumulative probability of all simulated CPFs. This approach is similar to normalization by a CPF of equally distributed ages [86], but also takes the likelihood of sampling into account.

2.3.4. CPF-Based 'Sedimentation Rate'

To account for further sampling biases (e.g., samples from a specific period preferably sampled), we also took the depth of the ^{14}C-ages into account. Therefore, we randomly sampled depths from all sediment sequences and simulated a possible age of the sediments a certain depth. The age probability function is a function of the overlying and underlying age in the sediment sequence. We sampled a calendar year from the age distribution of both the over- and underlying sample. Subsequently, one age is drawn from the range between both ages. The process is repeated 1000 times to get an age probability distribution for the random depth. Age distributions were calculated for 1000 random depths. From all simulated ages, a kernel density estimate is computed following the procedure proposed by Bevan and Crema [53]. This kernel density of ages is proportional to sedimentation rates. Additionally, the number of ages sampled in one simulation run is equal to the number of empirical ^{14}C-ages to calculate confidence intervals of the kernel densities and to take the original sample size into consideration.

2.3.5. Facies Change

At the random depths described above (Section 2.3.4), also the facies information given in the original publication of the sediment sequences was recorded. Thus, for all the different facies units, kernel densities of the possible ages were calculated.

3. Results

3.1. Cumulative Probability Functions

Cumulative probability functions of the available ^{14}C-ages from the western lower Bakırçay plain are depicted in Figure 3a–d.

3.1.1. Normalization

Except for a period between 2.3 ka BP and 2.8 ka BP, the CPFs of normalized and non-normalized ^{14}C-ages do not show major differences (Figure 3a). Around 2.7–2.8 ka BP, a distinct peak in the CPF of the normalized data can be observed that is not visible in the CPF of the non-normalized data. In the period after the peak, the cumulative probability of the non-normalized data is in contrast higher than the cumulative probability of the normalized data. This difference is due to a pronounced wiggle in the IntCal13 calibration curve around 2700–2500 ^{14}C-ages BP prior to the so-called Hallstatt-plateau (e.g., [98]). In the following, only non-normalized ages are described.

3.1.2. General Trends in the CPF

The CPF of all ages shows several changes in the cumulative probability, starting at 10.1 ka BP (Figure 3a). For several phases, the dating probability is zero (9.5–9.2 ka BP, 8.2–8.0 ka BP, 5.9–5.3 ka BP,

and 1.4–1.3 ka BP). Four major plateaus of increased cumulative probability are recorded (9.0–8.6 ka BP, 5.3–5.0 ka BP, 2.8–2.4 ka BP, and 2.0–1.6 ka BP). After 3.0 ka BP, the cumulative probability increases more or less continuously, reaching a maximum at around 1.7–1.6 ka BP. There is a marked depression in the CPF between 1.6 and 1.3 ka BP that is followed by a more or less continuous record until present.
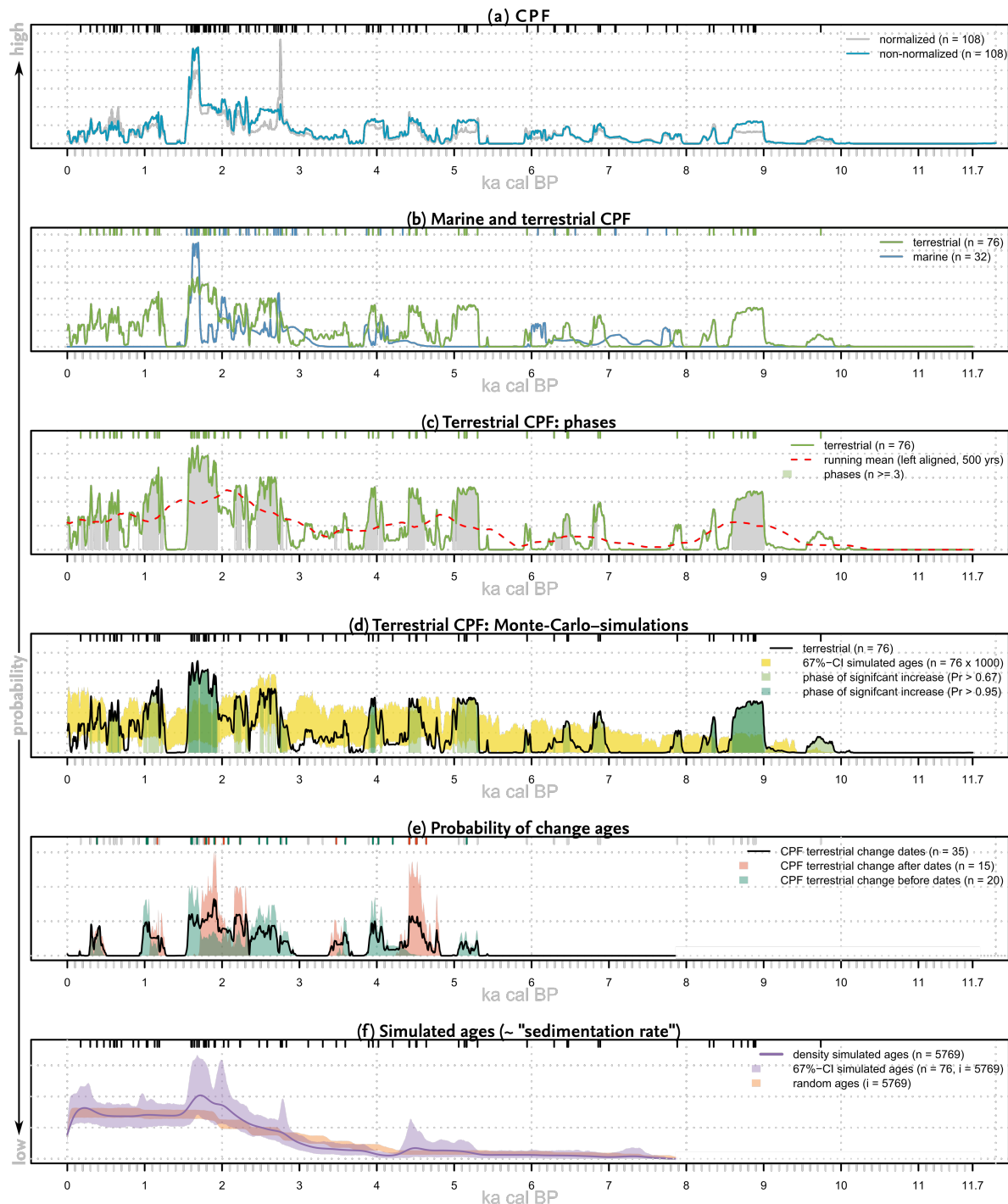
Figure 3. Cumulative probability functions and data from the null model calculated on the basis of different settings. Average normalized data of different archaeological periods are displayed in Figure 6. Stripes on the upper part of each plot show the median age of the relevant ages. The x-axis of all graphs show probabilities ranging from low to high. CI = confidence interval.

3.1.3. CPF of Terrestrial and Marine Ages

The CPFs of ^{14}C-ages sampled from terrestrial sediment layers and the CPF of ^{14}C-ages sampled from marine ages differ clearly (Figure 3b). This is especially true for the several peaks in the terrestrial CPF before 3 ka BP. While the earliest increase in the CPF of terrestrial ages is recorded for 10.1 ka BP, the CPF of marine ages first increases at 7.8 ka BP. Major phases of an increased CPF of terrestrial ages, viz. 9.0–8.6 ka BP, 5.3–5.0 ka BP, 4.6–4.4 ka BP, and 3.6–3.2 ka BP, are not equally evident in the marine record. In contrast, the CPF of the ages from marine sediment layers is higher than the terrestrial CPF between 7.8 and 7.0 ka BP and between 6.2 and 6.0 ka BP. After 3 ka BP, the increase of the cumulative probability occurs more or less simultaneously in terrestrial and marine records. The CPF of the marine ages decreases after 2.0 ka BP and again peaks at around 1.7 ka BP. During this period, the cumulative probability of the terrestrial ages is continuously high. The cumulative probability of marine ages decreases to zero after 1.4 ka BP. For the following analysis, only the terrestrial ages are considered.

3.1.4. Phases of Increased Terrestrial Cumulative Probability

Statistically, nine phases of increased cumulative probability of terrestrial ages were detected (Figure 3c), viz. (i) between 9.0 and 8.6 ka BP, (ii) between 6.5 ka BP and 6.2 ka BP, (iii) between 5.4 ka BP and 5.0 ka BP, (iv) between 4.6 ka BP and 4.4 ka BP, (v) between 4.1 ka BP and 3.9 ka BP, (vi) between 2.7 and 2.4 ka BP, (vii) between 2.0 and 1.6 ka BP, (viii) between 1.2 and 1.0 ka BP, and (ix) between 0.7 and 0.1 ka BP. These phases all lasted more than 100 years; phases with an interruption of less than 100 years are aggregated. In these phases i–ix, the cumulative probability increased the 1000-years running mean of the cumulative probability (and at least the probability of three ages contributed to the cumulative probability during that phase). The running mean shows that the phase between 9.0 and 8.6 ka BP is followed by a super-ordinate phase of low mean cumulative probability, which lasted until 5.3 ka BP. On average, the cumulative probability tends to increase between 5.3 ka BP and 1.6 ka BP, but is interrupted by a phase of low mean cumulative probability between 3.8 ka BP and 2.8 ka BP.

3.1.5. Comparison with the Null Model

Most of the nine phases of increased cumulative probability are statistically significantly different from the null model (simulated CPFs) at 67% confidence (Figure 3d, yellow envelope and light green columns). Three phases are statistically significantly different from the null model at 95% confidence, viz the phase between 9.0 and 8.6 ka BP, the phase between 4.1–3.9 ka BP, and 2.0–1.6 ka BP (Figure 3d, dark green columns). For several time intervals, the cumulative probability is statistically significantly increased, but cumulative probabilities were calculated from the dating probabilities of less than 3 ages or are not higher than the 1000 years running average (e.g., at 8.4–8.3 ka BP or between 7.0 and 6.8 ka BP).

3.2. Cumulative Probability Functions of Change Ages

In total, 35 terrestrial change-ages are available from the sediment sequences, indicating change after ($n = 15$) or change before ($n = 20$) the given age (Figure 3e). The CPFs of the change-after and change-before ages point to several phases of variation in deposition style; before 4.8 ka BP, the CPF of change-ages is not congruent to the CPF of all terrestrial ages but is especially similar after 2.8 ka BP. No-change ages are recorded before 5.4 ka BP; a single change-age dates between 5.4 and 5.0 ka BP.

A phase of change-after ages is recorded for between 4.8 ka BP and 4.2 ka BP, transitioning into a phase of change-before ages between 4.4 ka BP and 3.9 ka BP. Thus, the change-ages point to a change in sedimentation style between 4.4 ka BP and 4.1 ka BP. A phase of overlapping change-before and change-after between 3.7 ka BP and 3.4 ka BP does not point to a specific phase of change. Between 2.9 ka BP and 2.4 ka BP, only the cumulative probability of change-before ages is increased. The cumulative probability of change-after ages increases after 2.5 ka BP. Between 2.5 and 1.7 ka BP, the cumulative probability of change-after ages is higher than the cumulative probability of change-before ages. Between 1.7 and 1.5 ka BP, only change-before ages are recorded, followed

by a phase of no-change ages. The latest marked phase of change-ages is recorded between 1.4 and 1.0 ka BP (change-after ages between 1.4 and 1.1 ka BP and a change-before ages between 1.1 and 1.0 ka BP.)

3.3. Sedimentation Rate

The sedimentation rate calculated based on CPFs of estimated ages at random depths points to five distinct phases of higher and lower sedimentation dynamics compared to the null model (Figure 3f). The modeled sedimentation rate is relatively constant at a low level between 10.1 ka BP and 5.4 ka BP. During this period, the mean simulated CPFs of the age-depth model does not exceed the null model (CPF of ages randomly distributed over the sediment sequences) except of the period between 7.5 and 7.1 ka BP, where the 95% confidence interval of the simulated ages increases the confidence interval of the random ages.

The 95% confidence interval of the simulated ages also increases the confidence interval of the null model between 5.1 and 4.3 ka BP and between 2.9 ka BP and present, indicating increased sedimentation rates.

Between 4.2 and 1.7 ka BP, the simulated sedimentation rate constantly increased; the average of the simulated CPF exceeds the null model between 2.3 ka BP and 1.7 ka BP. After 1.5 ka BP, the sedimentation rate is not increased.

3.4. Facies Change

Several phases of a marked change in the terrestrial facies of the sediment sequences can be identified (Figure 4). The most pronounced change in facies occurred around 7.1 ka BP; being, however, only covered by a small number of dates and possibly due to terminological differences between the original publications. The decreasing proportion of overbank and channel-related sediments and an increase in fluvial sediments might not necessarily point to an absolute change in the depositional environment. The changes in the facies composition at around 6.3 ka BP and 5.8 ka BP are characterized by a decrease of sediments indicating coastline propagation. At around 4.2 ka BP, the proportion of sediments forming alluvial fans and sediments indicating a progradational depositional environment increases. After 2.7 ka BP, the proportion of colluvial sediment layers and overbank sediments increases. At round 2.0 ka BP the summed contribution of overbank, colluvial, and fan sediments reaches a local maximum; the contribution of channel-related sediments increases afterwards. The composition remains relatively stable with minor variations after 1.6 ka BP.
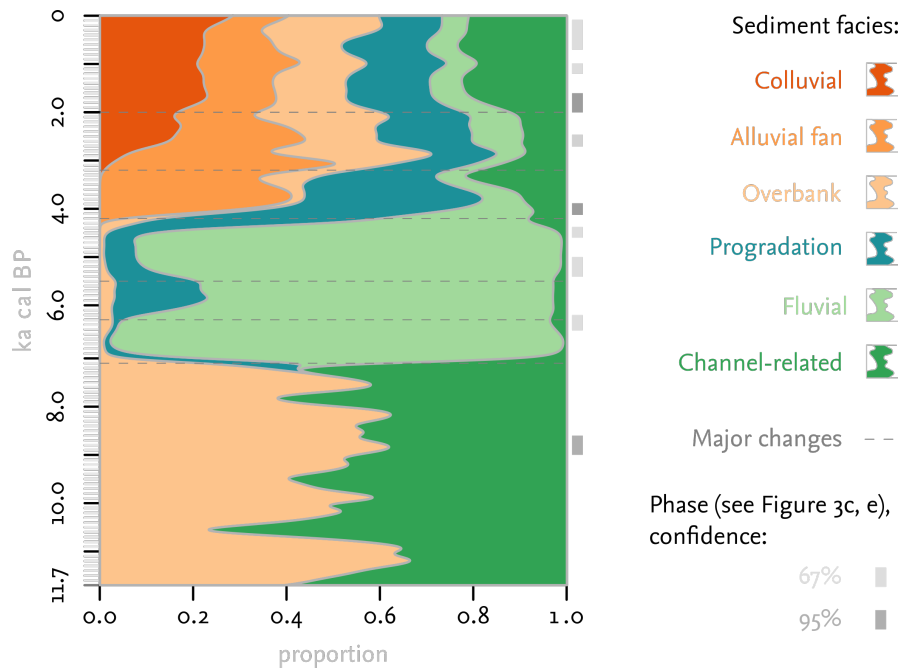
Figure 4. Modeled facies change (relative cumulative probability functions of estimated ages of sediment layers associated with different facies). Facies terminology is taken from the original publication and is thus not always non-overlapping.

4. Discussion

4.1. Early Holocene (ca. 11.7–8.2 ka BP)–Aceramic Neolithic

Highest climatic erosion susceptibility in the eastern Mediterranean region after the Pleistocene presumably occurred during Early Holocene peaking around 10 ka BP (Figure 5m) [7], coinciding with an Early Holocene wet period in the Balkans and Anatolia (Figure 5n,o) [99]. During this period, rainfall erosivity was relatively high. This effect may be coupled with a relatively low vegetation cover after the dry late Glacial [100–102]. Notwithstanding the high erosion susceptibility during the Early Holocene, sediment dynamics were relatively low and mainly triggered by climate variability and concurrent environmental change. Human impact during Early Holocene was neglectable but increasing [103]. The distribution of farming and a west-ward human migration from the Fertile Crescent associated with the onset of Neolithisation caused an increase in population in Anatolia and the Balkans (Figure 5a,d), however without reaching the Aegean region before ca. 8.5 ka BP [103].
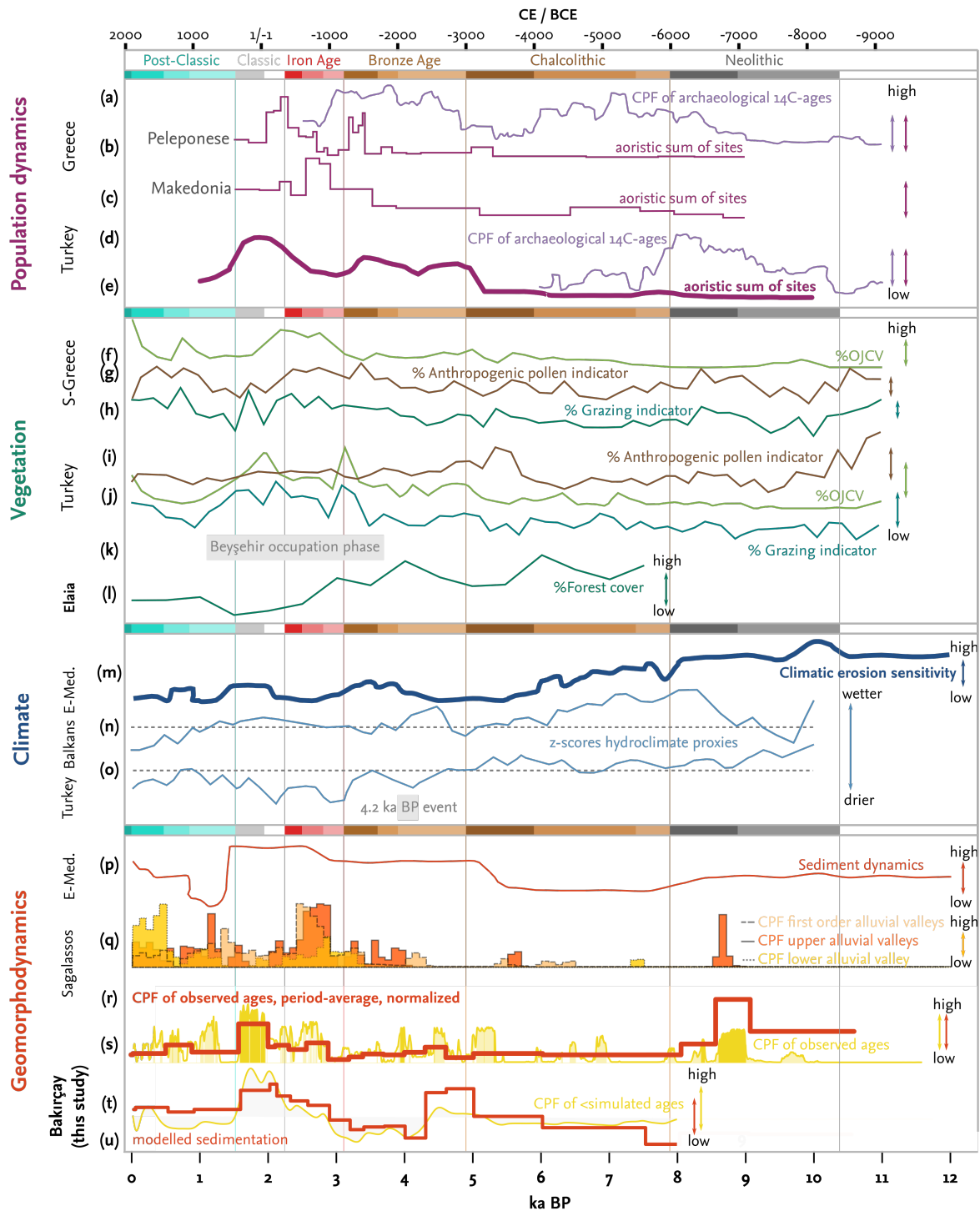
Figure 5. Comparison of the indicators for changing geomorphodynamics from this study in comparison with other archaeological/environmental proxies. Only relative values are shown. References: a: [104]; b, c: [105]; d: [104]; e: [106]; f, g, h: [105]; i, j: [106]; k: [107]; l: [41], interpolated; m: [7]; n, o: [99]; p: [7]; q: [8]; r–u: this study.

Our meta-analysis from the western lower Bakırçay plain shows one clear, statistically significant increase of the cumulative probability of ^{14}C-ages during the Early Holocene, ranging from 9.0 to 8.6 ka BP (Figure 5r) and thus coinciding with the Ceramic Neolithic [108,109]. As a result of lacking metadata for some of the ^{14}C-ages in our data set, we could not reliably estimate the sediment accumulation in

the western lower Bakırçay plain for the Early Holocene. Interpretations have therefore to be taken with caution.

The increased cumulative probability during that period in the western lower Bakırçay plain fit to the general trend of increased population dynamics and vegetation change in southeast Europe and Anatolia. In southern Greece, more clearly than in (Southern) Anatolia, palynological data show an increase in anthropogenic pollen indicator and grazing indicators (Figure 5g–i, [105,106]). Archaeological evidence points to the earliest known human activities around the western lower Bakırçay plain possibly between the 7th and the 5th millennium BCE (Late Ceramic Neolithic to Chalcolithic), although the settlement history might go back to the Aceramic Neolithic [110–112]. The prehistoric sites in the western lower Bakırçay plain are limited to the northern part of the plain and the Gümüş valley. The settlement cluster in the Gümüş valley (Figure 1) developed in the 5th and 4th millennium BCE [112]. The sediment sequences included in our data set are not located in the vicinity of these sites. Assuming a localized impact of the prehistoric sites, the contribution of an anthropogenic trigger to the increased cumulative probability before 8.6 ka BP is still unclear. Potentially above-average wetness (Figure 5n,o) during the phase may have also contributed to increased geomorphodynamics (cumulative probability of ^{14}C-ages). Berger et al. [113] show an increase in humidity during the period of increased geomorphodynamics that goes along with increased population dynamics. In studies on sediment dynamics in other regions of the eastern Mediterranean [7], the Early Holocene is relatively seldom covered. However, Fuchs et al. [9] reconstructed phases of increased sedimentation rates during the Neolithic on the Peloponnese peninsula (S-Greece); based on this data, Fuchs [55] concludes that Early Holocene sediment dynamics are related to both climate and human impact (i.e., high rainfall reconstructed form δ^{18}O values; archaeologically testified increase in settlement dynamics). Studies on the Çarşamba alluvial fan (Konya Basin, Central Anatolia), where the important site of Çatalhöyük is located, revealed an early human impact. Additionally around Sagalassos, a distinct peak in the CPF of alluvial sediments occurs [8], which coincides with the peak in cumulative probability in the western lower Bakırçay plain. Phases of increased soil erosion around Arslantepe (eastern Anatolia) partly overlap with the period reconstructed for the western lower Bakırçay plain. At Arslantepe, the increased geomorphodynamics occurred before the known onset of the settlement period; thus, also here climate might have triggered erosion [114].

4.2. Middle Holocene (ca. 8.2 to 4.2 ka BP)–Ceramic Neolithic to Late Chalcolithic

For the eastern Mediterranean region, the Middle Holocene can be characterized as a phase of more or less continuous decline or stability of the climatic erosion sensitivity [7]. In the Balkans, reconstructed hydroclimate followed a trend of continuous aridization from the wettest Holocene period around 8.0 ka BP [99] (Figure 5n) until ca. 4.9 ka BP.

In the area of modern Turkey, the aridization trend is less pronounced, but culminated in the so-called 4.2-ka-BP-drought-event [99] (Figure 5o) that dates to a period around 4.3/4.2–3.9/3.8 ka BP [115,116]. Estimated sediment dynamics in the eastern Mediterranean during the Mid-Holocene remained stable at a low level, but show a phase of increased dynamics between 5.5 and 5.0 ka BP [7] (Figure 5p). Human activities in Anatolia and Greece reconstructed from archaeological cumulative ^{14}C-ages and the aoristic sum of site counts (Figure 5a–e) first declined during the Mid-Holocene, but increased after 5.2 ka BP (Late Chalcolithic–Early Bronze Age), when also the estimated sedimentation dynamics increased [7] (Figure 5p).

The cumulative probability of ^{14}C-ages from sediment sequences and the reconstructed sedimentation in the western lower Bakırçay plain also increased during the aforementioned period (Figures 3 and 5r–u). An earlier peak in sediment dynamics occurred in the (Late) Chalcolithic (especially after 5.4 ka BP), followed by a more pronounced average increase in sediment dynamics during the Early Bronze Age. This increase is in accordance with the model for the entire eastern Mediterranean and also coincides with general changes in vegetation cover in the area of modern Turkey and Greece (Figure 5f–k). In the Aegean region of Anatolia, settlement activities also increased during the Late Chalcolithic; the number of archaeological sites in the area of modern Turkey

increased around 5.2 ka BP. The palynological record originating from the region shows an increase of anthropogenic pollen indicators (including a relative increase of OJCV-pollen and grazing indicator species) between 5.7 ka BP and 4.6 ka BP. The palynological record from the Bay of Elaia [41] close to the Bakırçay delta shows a reduction of forest cover during the period of increased geomorphodynamics.

Although an anthropogenic driver of increasing geomorphodynamics in the late Middle Holocene appears to be clear given the fact that human activities increased and palynological data indicates increased land-use pressure, changing hydro-climatic conditions (i.e., increased erosivity) cannot be excluded as a trigger. In the Balkans, a wet phase occurred between 4.6 and circa 4.0 ka BP [99] (Figure 5n). However, the hydro-climatic reconstructions from the area of modern Turkey indicate a wet phase between 5.4 and 4.4 ka BP [99] (Figure 5o).

In the western lower Bakırçay plain, the number of settlements increased from the Early–Middle Chalcolithic to the Late Chalcolithic–Early Bronze Age [110]. During this period the western lower Bakırçay plain was the first time continuously settled. This also implies that the increased geomorphodynamics were triggered by settlement activities. To what extent the reconstructed geomorphodynamic presented here are representative for the whole western lower Bakırçay plain has to be further surveyed. Some of the sediment sequences in our data set were obtained from locations in the vicinity of Late Chalcolithic–Early Bronze Age settlements, such as Elaia, Yeni Yeldeğirmintepe, and Başantepe. Neolithic sites were, however, not found in the vicinity of the locations of the sediment sequences. Therefore, not only the absolute increase in sites during the Late Chalcolithic but also the site pattern may have had an effect on the observed increase in geomorphodynamics.

4.3. Late Holocene (4.2 ka BP to Present)–Early Bronze Age to Post-Classic Period

According to the review analysis of Dusar et al. [7], the Late Holocene in the eastern Mediterranean is characterized by low climatic sensitivity to erosion, but high sediment dynamics. Thus, increased soil erosion and a subsequently increased deposition in the lowlands is not due to higher rainfall erosivity, but due to reduced land cover. Accordingly, palynological proxies from S-Anatolia and S-Greece document a high human impact on the vegetation cover (Figure 5f–k). Thus, human activity became a dominant factor triggering geomorphodynamics. In addition to the general trend of climatic sensitivty to erosion, hydro-climatic signal from the Balkans and the area of modern Turkey differ. Whereas in the area of modern Turkey pronounced dry phases are recorded, an increase in wetness in the neighboring Balkans is recorded for the period between 3.0 ka BP and ca. 1.2 ka BP (Figure 5m–o).

4.3.1. Early Bronze Age to Iron Age

The reconstructed geomorphodynamics in the western lower Bakırçay plain decreased at the beginning of the Late Holocene. This is especially evident in the decline of the modeled sedimentation rate after 4.3 ka BP (Figure 5u). In addition, the cumulative probability of change-ages point to marked sediment facies change during that period (Figure 3e). The marked change in geomorphodynamics at the transition from the Middle to the Late Holocene is distinctly related to climatic variations: The so-called 4.2-ka-BP-drought-event caused a decline in settlement activities in the eastern Mediterranean (Figure 5a,e) and elsewhere around the Mediterranean Sea [117–121]); from Central Anatolia, it is well documented that many sites were abandoned [122]. The collapse of Mediterranean civilizations might also been fostered by the drought event [115,116,123].

In the western lower Bakırçay plain, an 800-year gap in occupation is recorded as from the end of the Early Bronze Age. During this period, the forest cover around Elaia on the coastal fringe of the western lower Bakırçay plain increased (Figure 5l).

The modeled sedimentation in the western lower Bakırçay plain remained on a relatively low level from the beginning of the Late Holocene (4.2 ka BP) until 3.3–3.2 ka BP. Although there is an increase in the cumulative probability of ^{14}C-ages directly after 4.2 ka BP, the observed CPF tendentiously remains on a low level until 2.7 ka BP (Figure 5r,s).

After ca. 3 ka BP, geomorphodynamics in the western lower Bakırçay plain markedly increased, coinciding with a phase of low climatic erosion sensitivity and a general trend in increasing human activities that is also documented by an increase in palynological indicators for human activity (Figure 5). The effect of settlement activities on geomorphodynamics is reflected by a relative increase in colluvial sediments after 3 ka BP (Figure 4). The period between 3.2 and 1.5 ka BP is known as the Beyşehir Occupation Phase in Anatolia. This phase was identified from a pollen diagram originating from southwestern Anatolia [107]. The meta-analysis of Woodbridge et al. [106] showed an increase in OJCV-pollen and grazing indicator species in Anatolia during the Beyşehir occupation phase. Pollen data indicate a contemporaneous decrease in forest cover around the Bay of Elaia (Figure 5l).
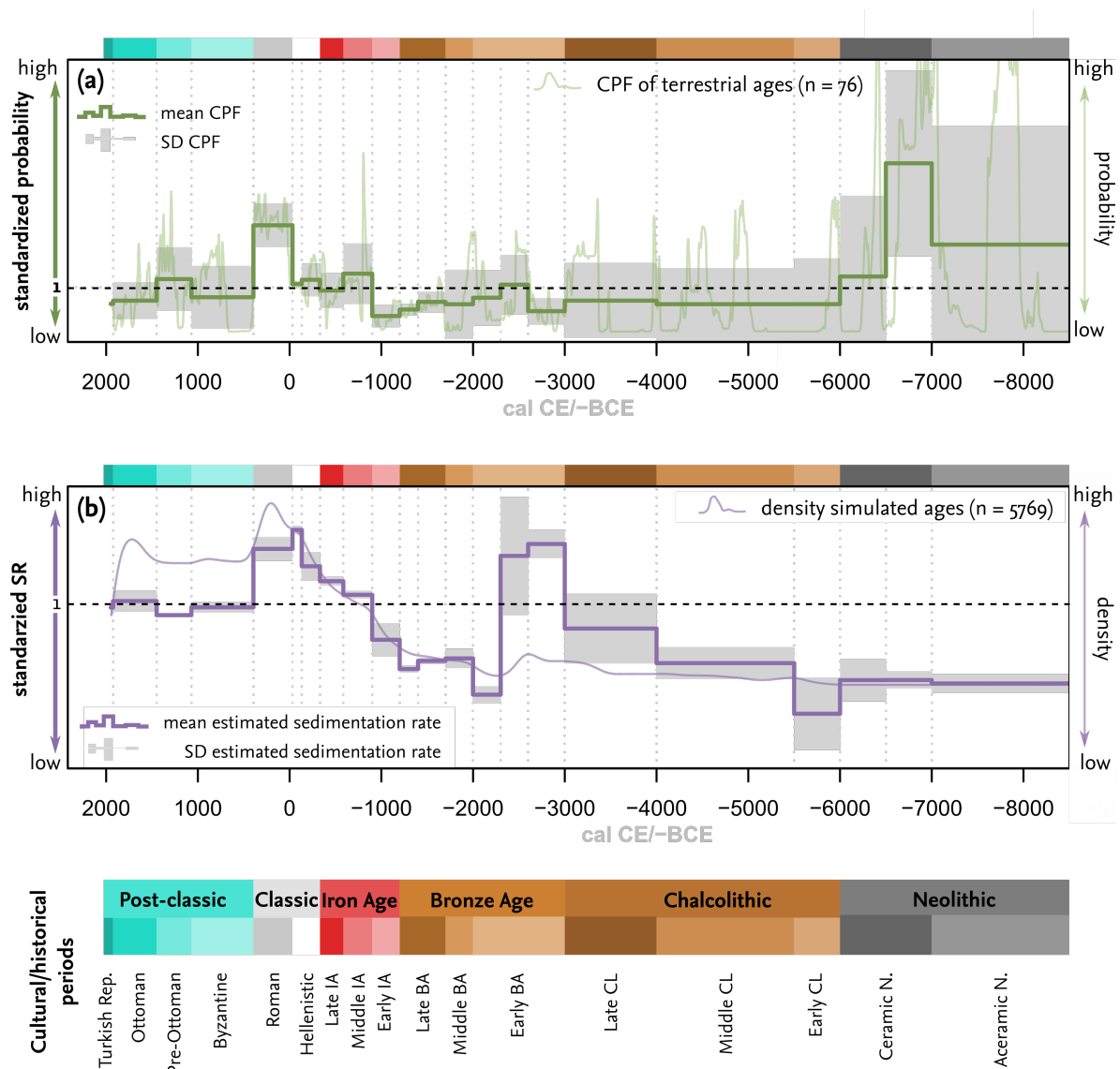
Not only in the western lower Bakırçay plain, but also in other regions in Anatolia, geomorphodynamics increased around 3 ka BP [8,114,124,125]. In the surroundings of the ancient city of Sagalassos in Southern Anatolia, geomorphodynamics increased simultaneously to a phase of increased deforestation and intensified cultivation and pastoralism [126,127].

4.3.2. Classic and Post-Classic Period(s)

Modeled sedimentation in the western lower Bakırçay plain peaks between 2.1 and 1.6 ka BP; the cumulative probability of ^{14}C-ages is the highest after 2.0 ka BP; change-ages point to facies change around the same time (Figure 3). Thus, geomorphodynamics were high during the Classical period, reaching a maximum during Roman Imperial times (Figure 6).

From an archaeological point of view, the transition from Hellenistic to Roman Imperial times is of special interest, as it is associated with a marked change in the settlement pattern in the western lower Bakırçay plain and a population increase in the major city of Pergamon. After the Eumenian expansion of Pergamon in the 2nd century BCE [128], the population density in the micro-region decreased, but the population in the cities of Pergamon and Elaia increased [128]. The city area of Pergamon quadrupled in the 2nd century BCE [129]. The area of the lower city further grew under the reign of Trajan (98–117 CE), including the location of residential quarters, major buildings, and bathes in the surroundings. In the 2nd century BCE, also the city of Elaia grew [128].

Although the sediment sequences were not obtained from the direct vicinity of the city of Pergamon, the Hellenistic–Roman transformation might have also affected remote areas in the micro-region. Historical reports (Galen, 5, 49) imply that around 180,000 people lived in the Pergamon Micro-Region in the 2nd century BCE. Population estimates based on historical architecture indicate a number of circa 34,000 people that lived in the city of Pergamon during that time [129]. Between Hellenistic and Roman Imperial times, the city area increased from circa 110 ha to circa 230 ha [129]. From approximations, it can be presumed that an important portion of the micro-region was under utilization to supply the urban and rural population of Pergamon and its micro-region in the 2nd century CE [14,130,131]. Although timber for the urban building program was felled. (Alternatively, large-scale imports would have been required.) Palynological data from Elaia indicate a relatively sparse forest cover during that period [41]. Although vegetation dynamics in the area of modern Turkey are well correlated with climate fluctuations [104], it is reasonable to assume that the high demand for food is a significant driver of forest cover reduction in the western lower Bakırçay plain. The dryness in the area of modern Turkey (Figure 5)—and therefore a reduced vegetation cover—might have enhanced and accelerated the effect of human activities that lead to the increased geomorphodynamics since 2.0 ka BP.

Figure 6. (**a**) Cumulative probability function (CPF) and (**b**) average sedimentation rate of sediment sequences obtained from the western lower Bakırçay plain. Both data are normalized based on the null model and are averaged over archaeological periods (bold lines; see Table A1); also the non-normalized data are displayed, as shown in Figure 3. Grey backgrounds indicate the variability within the archaeological period. The dashed lines indicated no difference between the observed data and the null model. SD = standard deviation, SR = sedimentation rate, N = Neolithic, CL = Chalcolithic, BA = Bronze Age, IA = Iron Age.

In accordance with our findings, data from sediments from the Bay of Elaia reported by Seeliger and co-authors indicate increased erosion during this time in the catchments around the city of Elaia (after 2.7–2.6 ka BP [41]; around 2.3–2.2 ka BP [37]). Schneider and co-authors did not, however, observe an increase in sediment dynamics during the Classical period analyzing single sediment sequences from the western lower Bakırçay plain [48,49]; they invoke terraces as a factor that minimized soil erosion processes during Roman Imperial times around the city of Atarneus [49]. We, however, observed a decline in geomorphodynamics after Roman Imperial times. Failures of terraces might thus not have caused increased erosion [132,133].

The increased geomorphodynamics during the Classic period appears more or less ubiquitously in the Aegean region [7,30,81,114,134–137]. By contrast, the reconstructed sediment dynamics in the surroundings of Sagalassos [8] peaked during the Iron Age, before the major settlement phase in the

Classic period and the related intensive land use [138]. Thus, the peak in sediment dynamics around Sagalassos appeared during the increase in human pressure on the landscape, but not during the heydays of the city when human pressure was presumably on its maximum. By contrast, sediment dynamics in the western lower Bakırçay plain, rather increased with increasing human activities. Several aspects may explain the differences in the development of the micro-regions of Sagalassos and Pergamon, including (i) the general variability in the record; (ii) the difference in location of the sediment sequences concerning sediment sinks or sources (sediments from valley fills vs. colluvial/fan sediments; vicinity to the coast in the western lower Bakırçay plain); (iii) soil conservation measures such as terracing [49]), or (iv) variability in landscape sensitivity to erosion, resilience, or trigger–reaction delays. Dusar et al. [8] analyze different colluvial and fluvial archives, whereas the sediments in our data set are mainly obtained from colluvial deposits or low order catchments. Archives from colluvial deposits or low order catchments reflect human disturbance more directly than alluvial deposits of larger drainage systems [8,10,139,140]. The signal from sediment archives obtained from the floodplain of higher order catchments—thus topographically lower compartments of the sediment cascade—are more likely affected by a time lack. The resilience time in e.g., colluvial archives is therefore much lower than in floodplain sediments.

Soil depletion [16] and a decreased erodibility due to higher stone coverage of soils after a period of erosion during the Iron Age around Sagalassos are a reason why geomorphodynamics might peak before the climax in human activities during the Classic period [12,141]. The depletion of soils on slopes that were sensitive to erosion might have caused a shift of agricultural activities and settlement locations to plain areas around Sagalassos that were less susceptible to erosion [12]. Preliminary data of Knitter and Ludwig [142] on the archaeological site distribution pattern in the Pergamon Micro-Region indicate a change of the preferred locations in the Classic period. While the preferred settlement location before Roman Imperial times were on summits, they moved to slopes during Roman Imperial times. Based on the available data, it can be inferred that Roman Imperial sites were located in places characterized by higher soil erosion sensitivity compared to older sites. This might also explain the increase in sediment dynamics recorded for the western lower Bakırçay plain from Hellenistic to Imperial times.

After Roman Imperial times, geomorphodynamics decreased in the western lower Bakırçay plain. Changes from the dominance of arable farming to animal husbandry around Elaia [41] might have been local. Rather, the decline in geomorphodynamics is attributed to an overall decline in human activities in the western lower Bakırçay plain.

The geomorphodynamics in the post-Classic periods are not further discussed in the paper, as archaeological research in the area focused on Prehistoric to Classic periods.

5. Conclusions

Data from sediment sequences obtained from the western lower Bakırçay plain were examined concerning geomorphodynamics mainly based on cumulative probability functions of ^{14}C-ages. We, therefore, modified current approaches to cope with certain biases in the data by comparing observed cumulative probabilities with simulated probabilities and by estimating sediment accumulation.

Both, cumulative probability functions and modeled sediment accumulation points to several phases of increased geomorphodynamics that were not identified in the analysis of single sequences. Inference statistics show that during these phases geomorphodynamics are statistically significantly different from randomly distributed data. Thus, although the number of samples in our data set (76 terrestrial ages) is limited compared to supra-regional studies, we obtained reasonable results that help to further understand human–environment interactions in the western lower Bakırçay plain.

Several aspects can be highlighted:

- Phases of increased or reduced geomorphodynamics in the western lower Bakırçay plain follow the general trend of sediment dynamics in the eastern Mediterranean.

- The development of local geomorphodynamics is in good agreement with the changing hydro-climatic conditions as well as vegetation and population dynamics in Anatolia, Greece and the neighboring Balkan region.
- From this coincidence, climatic triggers of geomorphodynamics appear to be (most) important in the Early Holocene, prior to Holocene aridization. However, the Early Holocene phase of increased geomorphodynamics coincided with the potential onset of early settlement activities in the western lower Bakırçay plain. Thus, relatively low human impact may have (even marginally) contributed to increased geomorphodynamics in the area—conceivably due to a general high sensitivity of the landscape to erosion. The decrease in geomorphodynamics in the western lower Bakırçay plain at the end of the middle Holocene is related to a climatic event, i.e., the 4.2-ka-BP-drought-event. This drought event caused widespread settlement abandonment and a decrease in population in Anatolia.
- Geomorphodynamics in the western lower Bakırçay plain peaked during the Classic period. The transformation of the Pergamon Micro-Region from Hellenistic to Roman Imperial times included urbanization and demographic growth, which most likely were the most important triggers of increased geomorphodynamics.
- Geomorphodynamics in the western lower Bakırçay plain and many other areas in Anatolia show a similar trend. Nonetheless, major differences in the Classical periods occurred. Whereas geomorphodynamics and settlement activities in the western lower Bakırçay plain are entangled, this is not the case in other major cities in Anatolia, such as Sagalassos. The reasons for the difference might either be related to differences between the sediment archives or diverging landscape sensitivities and land use dynamics.

To better understand the difference in geomorphodynamics and to overcome the simplicity of interpretations mainly based on synchronicity of geomorphodynamics and general trends in human activities and climate variability, further research on the entanglement of local geomorphodynamics and settlement dynamics is required. This especially includes the understanding of geomorphodynamics in the Early Holocene and studies on the cause–effect relationships between settlement activity and varying geomorphodynamics in the western lower Bakırçay plain [143]. This should include the modeling of past soil erosion to overcome the bias of location of the sediment sequences in the vicinity of settlements of a distinct period and the general problem of the spotty nature of sediment sequences. Evaluating the relationship between archaeological site patterns and landscape sensitivity to erosion, soil conservation measures, and studies that are not related to archaeological sites of a specific period might provide further insights in human-environment interactions in the western lower Bakırçay plain. In addition, palynological or phytolith studies might improve the understanding of agricultural use in the area.

Irrespective of the potential shortcomings of a meta-analysis, we conclude that our study reveals the general interrelationship of settlement history and geomorphodynamics in the western lower Bakırçay plain, especially the human-inducted climax of geomorphodynamcis in Roman Imperial times.

Author Contributions: Conceptualization, F.B. and B.S.; methodology, F.B.; software, F.B.; validation, F.B., D.K., M.N., and B.S.; formal analysis, F.B., M.N.; investigation, F.B., M.N.; resources, B.S.; data curation, F.B. and M.N.; writing—original draft preparation, F.B.; writing—review and editing, D.K., M.N., B.S.; visualization, F.B.; supervision, D.K., B.S.; project administration, F.B., B.S., D.K.; funding acquisition, D.K., B.S. All authors have read and agreed to the published version of the manuscript.

Abbreviations

The following abbreviations are used in this manuscript:

BA	Bronze Age
CI	Confindence Interval
CL	Chalcolithic
CPF	Cumulative probability function
IA	Iron Age
N	Neolithic
OJCV	*Olea, Juglans, Castanea, Vitis*
SR	Sedimentation rate

Appendix A

Appendix A.1

Table A1. Overview on the archaeological periods as used in this study. Periodisation is based on [106,109,128,144]

Period	Subperiod	Chronology [-BCE/CE]
Neolithic	Aceramic Neolithic	−8500 to −7000
	Early Ceramic Neolithic	−7000 to −6500
	Late Ceramic Neolithic	−6500 to −6000
Chalcolithic	Early Chalcolithic	−6000 to −5500
	Middle Chalcolithic	−5500 to −4000
	Late Chalcolithic	−4000 to −3000
Early Bronze Age	EBA I	−3000 to -2600
	EBA II	−2600 to −2300
	EBA III	−2300 to −2000
Middle Bronze Age	MB1, MB2	−2000 to −1700
Late Bronze Age	LB1	−1700 to −1400
	LB2	−1400 to −1200
Iron Age	Early Iron Age	−1200 to −900
	Middle Iron Age	−900 to −585
	Late Iron Age	−585 to −331
Classic period	Hellenistic (Pergamenian Kingdom)	−331 to −133
	Hellenistic	−133 to −31
	Roman Imperial	−31 to 395
Late Roman/Byzantine	*Late Roman/Byzantin*	395 to 1071
Medieval/Modern	Pre-Ottoman	1071 to 1450
	Ottoman	1450 to 1923
	Turkish	1923 to 1950

Appendix A.2

Sedimentation rates used to estimate the cumulative probability functions of the null model are calculated as follows:

$$SR_i = \frac{d_i}{t_i} \tag{A1}$$

where SR_i is the sedimentation rate related to a ^{14}C-age i, d_i is the sampling depth of the age, and t_i is the median date of the dating likelihood of the age.

Taking the sedimentation rate, the maximum age of a sediment sequences is estimated (if only one date is available for a sequence; $n_{i,j} = 1$):

$$t_{d_{max,j}} = \frac{d_{max,j}}{SR_i} \tag{A2}$$

where $t_{d_{max,j}}$ is the maximum age of the sediment sequence j and $d_{max,j}$ is the thickness of sediment sequence j.

For sediment sequences with more than one ^{14}C-age available, we used a power function to estimate the maximum age:

$$t_{d_{max,j}} = d_{max,i}^{e_j} \tag{A3}$$

where e_j is the power calculated by a nonlinear least squares method applied to all ^{14}C-ages available from a sediment sequence. The general form of the equation is:

$$t_{i,est.} = d_i^e \tag{A4}$$

References

1. Vita-Finzi, C. *The Mediterranean Valleys: Geological Changes in Historical Times*; Cambridge University Press: Cambridge, UK, 1969.
2. Vita-Finzi, C. Solar history and paleohydrology during the last two millennia. *Geophys. Res. Lett.* **1995**, *22*, 699–702. [CrossRef]
3. Andel, T.H.V.; Zangger, E.; Demitrack, A. Land Use and Soil Erosion in Prehistoric and Historical Greece. *J. Field Archaeol.* **1990**, *17*, 379–396. [CrossRef]
4. Bintliff, J. Time, process and catastrophism in the study of Mediterranean alluvial history: A review. *World Archaeol.* **2002**, *33*, 417–435. [CrossRef]
5. Hughes, J.D.; Thirgood, J.V. Deforestation, Erosion, and Forest Management in Ancient Greece and Rome. *J. For. Hist.* **1982**, *26*, 60–75. [CrossRef]
6. Ackermann, O.; Greenbaum, N.; Ayalon, A.; Bar-Matthews, M.; Boaretto, E.; Bruins, H.J.; Cabanes, D.; Horwitz, L.K.; Neumann, F.H.; Porat, N.; et al. Using palaeo-environmental proxies to reconstruct natural and anthropogenic controls on sedimentation rates, Tell es-Safi/Gath, eastern Mediterranean. *Anthropocene* **2014**, *8*, 70–82. [CrossRef]
7. Dusar, B.; Verstraeten, G.; Notebaert, B.; Bakker, J. Holocene environmental change and its impact on sediment dynamics in the Eastern Mediterranean. *Earth-Sci. Rev.* **2011**, *108*, 137–157. [CrossRef]
8. Dusar, B.; Verstraeten, G.; D'haen, K.; Bakker, J.; Kaptijn, E.; Waelkens, M. Sensitivity of the Eastern Mediterranean geomorphic system towards environmental change during the Late Holocene: A chronological perspective. *J. Quat. Sci.* **2012**, *27*, 371–382. [CrossRef]
9. Fuchs, M.; Lang, A.; Wagner, G.A. The history of Holocene soil erosion in the Phlious Basin, NE Peloponnese, Greece, based on optical dating. *Holocene* **2004**, *14*, 334–345. [CrossRef]
10. Fuchs, M.; Zöller, L. Geoarchäologie aus geomorphologischer Sicht Eine konzeptionelle Betrachtung (Geoarchaeology from a Geomorphological Perspective—A Conceptual Consideration). *Erdkunde* **2006**, *60*, 139–146. [CrossRef]
11. Zolitschka, B.; Behre, K.E.; Schneider, J. Human and climatic impact on the environment as derived from colluvial, fluvial and lacustrine archives—Examples from the Bronze Age to the Migration period, Germany. *Quat. Sci. Rev.* **2003**, *22*, 81–100. [CrossRef]
12. Verstraeten, G.; Broothaerts, N.; Van Loo, M.; Notebaert, B.; D'Haen, K.; Dusar, B.; De Brue, H. Variability in fluvial geomorphic response to anthropogenic disturbance. *Geomorphology* **2017**, *294*, 20–39. [CrossRef]
13. Goodchild, H. Modelling Roman Demography and Urban Dependency in Central Italy. *Theor. Rom. Archaeol. J.* **2006**, 42–56. [CrossRef]

14. Hughes, R.E.; Weiberg, E.; Bonnier, A.; Finné, M.; Kaplan, J.O. Quantifying Land Use in Past Societies from Cultural Practice and Archaeological Data. *Land* **2018**, *7*, 9. [CrossRef]

15. Knitter, D.; Günther, G.; Hamer, W.B.; Keßler, T.; Seguin, J.; Unkel, I.; Weiberg, E.; Duttmann, R.; Nakoinz, O. Land Use Patterns and Climate Change—A Modeled Scenario of the Late Bronze Age in Southern Greece. *Environ. Res. Lett.* **2019**. [CrossRef]

16. Van Loo, M.; Dusar, B.; Verstraeten, G.; Renssen, H.; Notebaert, B.; D'Haen, K.; Bakker, J. Human induced soil erosion and the implications on crop yield in a small mountainous Mediterranean catchment (SW-Turkey). *CATENA* **2017**, *149*, 491–504. [CrossRef]

17. D'Haen, K.; Verstraeten, G.; Dusar, B.; Degryse, P.; Haex, J.; Waelkens, M. Unravelling changing sediment sources in a Mediterranean mountain catchment: A Bayesian fingerprinting approach. *Hydrol. Process.* **2013**, *27*, 896–910. [CrossRef]

18. Kaniewski, D.; Paulissen, E.; De Laet, V.; Dossche, K.; Waelkens, M. A high-resolution Late Holocene landscape ecological history inferred from an intramontane basin in the Western Taurus Mountains, Turkey. *Quat. Sci. Rev.* **2007**, *26*, 2201–2218. [CrossRef]

19. D'Haen, K.; Dusar, B.; Verstraeten, G.; Degryse, P.; De Brue, H. A sediment fingerprinting approach to understand the geomorphic coupling in an eastern Mediterranean mountainous river catchment. *Geomorphology* **2013**, *197*, 64–75. [CrossRef]

20. Kraft, J.C.; Kayan, İ.; Erol, O. Geomorphic Reconstructions in the Environs of Ancient Troy. *Science* **1980**, *209*, 776–782. [CrossRef]

21. Brückner, H. Coastal changes in western Turkey; rapid delta progradation in historical times. *Bull. L'Institut Oceanogr. Monaco-Spec.* **1997**, *18*, 63–74.

22. Brückner, H.; Müllenhoff, M.; Handl, M.; van der Borg, K. Holocene landscape evolution of the Büyük Menderes alluvial plain in the environs of Myous and Priene (Western Anatolia, Turkey). *Z. Geomorphol. NF* **2002**, *127*, 47–65.

23. Kraft, J.C.; Kayan, İ.; Brückner, H.; Rapp, G.R. Sedimentary Facies Patterns and the Interpretation of Paleogeographies of Ancient Troia. In *Troia and the Troad*; Wagner, G.A., Pernicka, E., Uerpmann, H.P., Eds.; Natural Science in Archaeology; Springer: Berlin/Heidelberg, Germany, 2003; pp. 361–377. [CrossRef]

24. Kraft, J.; Kayan, İ.; Luce, J. Harbor areas at ancient Troy: Sedimentology and geomorphology complement Homer's Iliad. *Geology* **2003**, *31*. [CrossRef]

25. Brückner, H.; Vött, A.; Schriever, A.; Handl, M. Holocene delta progradation in the eastern Mediterranean–Case studies in their historical context. *Méditerr. Rev. Géogr. Pays Méditerr. J. Mediterr. Geogr.* **2005**, *104*, 95–106. [CrossRef]

26. Brückner, H.; Müllenhoff, M.; Vött, A.; Gehrels, R.; Herda, A.; Knipping, M.; Gehrels, W.R. From archipelago to floodplain-Geographical and ecological changes in Miletus and its environs during the past six millennia (Western Anatolia, Turkey). *Z. Geomorphol. Suppl.* **2006**, *142*, 63–83.

27. Knipping, M.; Müllenhoff, M.; Brückner, H. Human induced landscape changes around Bafa Gölü (western Turkey). *Veg. Hist. Archaeobot.* **2008**, *17*, 365–380. [CrossRef]

28. Stock, F.; Kerschner, M.; Kraft, J.C.; Pint, A.; Frenzel, P.; Brückner, H. The palaeogeographies of Ephesos (Turkey), its harbours, and the Artemision–A geoarchaeological reconstruction for the timespan 1500–300 BC. *Z. Geomorphol. Suppl. Issues* **2014**, 33–66. [CrossRef]

29. Delile, H.; Blichert-Toft, J.; Goiran, J.-P.; Stock, F.; Arnaud-Godet, F.; Bravard, J.P.; Brückner, H.; Albarède, F. Demise of a harbor: A geochemical chronicle from Ephesus. *J. Archaeol. Sci.* **2015**, *53*, 202–213. [CrossRef]

30. Stock, F.; Knipping, M.; Pint, A.; Ladstätter, S.; Delile, H.; Heiss, A.G.; Laermanns, H.; Mitchell, P.D.; Ployer, R.; Steskal, M.; et al. Human impact on Holocene sediment dynamics in the Eastern Mediterranean–the example of the Roman harbour of Ephesus. *Earth Surf. Process. Landf.* **2016**, *41*, 980–996. [CrossRef]

31. Stock, F.; Seyer, M.; Symanczyk, A.; Uncu, L.; Brückner, H. On the geoarchaeology of Limyra (SW Anatolia)—New insights into the famous Lycian city and its environs. *Geoarchaeology* **2020**, *35*, 487–502. [CrossRef]

32. Vött, A.; Brückner, H.; Kraft, J.C. Do mythological traditions reflect past geographies? The Acheloos delta (Greece) and the Artemision (Turkey) case studies. *Z. Geomorphol. Suppl. Issues* **2017**, 203–221. [CrossRef]

33. Stock, F.; Halder, S.; Opitz, S.; Pint, A.; Seren, S.; Ladstätter, S.; Brückner, H. Late Holocene coastline and landscape changes to the west of Ephesus, Turkey. *Quat. Int.* **2019**, *501*, 349–363. [CrossRef]

34. Pirson, F. Elaia, der (maritime) Satellit Pergamons. In *Häfen und Hafenstädte im östlichen Mittelmeerraum von der Antike bis in Byzantinische Zeit: Neue Entdeckungen und Aktuelle Forschungsansätze = Harbors and Harbor Cities in the Eastern Mediterranean from Antiquity to the Byzantine Period: Recent Discoveries and Current Approaches, Istanbul, 30.05.-01.06.2011*; Number 19 in Byzas; Ladstätter, S., Pirson, F., Schmidts, T., Eds.; Zero Prod.: Istanbul, Turkey, 2014; pp. 339–356.

35. Pirson, F.; Ateş, G.; Bartz, M.; Brückner, M.; Feuser, S.; Mania, U.; Meier, L.; Seeliger, M. Elaia: Eine aiolische Polis im Dienste der hellenistischen Residenzstadt Pergamon? In *Urbane Strukturen und büRgerliche Identität im Hellenismus*; Number 5 in Hellenistische Polis als Lebensform; Matthaei, A., Zimmermann, M., Eds.; Verlag Antike: Mainz, Germany, 2015; pp. 22–55.

36. Seeliger, M. Elaia, the Maritime Harbour City of Ancient Pergamon (Turkey) ? Coastal Evolution and Human Impact over the Past Eight Millennia. Ph.D. Dissertation, Mathematisch-Naturwissenschaftliche Fakultät, Universität zu Köln, Zürich, Switzerland, 2016.

37. Seeliger, M.; Pint, A.; Feuser, S.; Riedesel, S.; Marriner, N.; Frenzel, P.; Pirson, F.; Bolten, A.; Brückner, H. Elaia, Pergamon's maritime satellite: The rise and fall of an ancient harbour city shaped by shoreline migration. *J. Quat. Sci.* **2019**, *34*, 228–244. [CrossRef]

38. Seeliger, M.; Pint, A.; Frenzel, P.; Feuser, S.; Pirson, F.; Riedesel, S.; Brückner, H. Foraminifera as markers of Holocene sea-level fluctuations and water depths of ancient harbours—A case study from the Bay of Elaia (W Turkey). *Palaeogeogr. Palaeoclimatol. Palaeoecol.* **2017**, *482*, 17–29. [CrossRef]

39. Seeliger, M.; Bartz, M.; Erkul, E.; Feuser, S.; Kelterbaum, D.; Klein, C.; Pirson, F.; Vött, A.; Brückner, H. Taken from the sea, reclaimed by the sea: The fate of the closed harbour of Elaia, the maritime satellite city of Pergamum (Turkey). *Quat. Int.* **2013**, *312*, 70–83. [CrossRef]

40. Pint, A.; Seeliger, M.; Frenzel, P.; Feuser, S.; Erkul, E.; Berndt, C.; Klein, C.; Pirson, F.; Brückner, H. The environs of Elaia's ancient open harbour – a reconstruction based on microfaunal evidence. *J. Archaeol. Sci.* **2015**, *54*, 340–355. [CrossRef]

41. Shumilovskikh, L.S.; Seeliger, M.; Feuser, S.; Novenko, E.; Schlütz, F.; Pint, A.; Pirson, F.; Brückner, H. The harbour of Elaia: A palynological archive for human environmental interactions during the last 7500 years. *Quat. Sci. Rev.* **2016**, *149*, 167–187. [CrossRef]

42. Kayan, İ.; Vardar, S. The physical geography of the Madra River Delta. In *The Madra River Delta: Regional Studies on the Aegean Coast of Turkey 1*; Lambrianides, K., Spencer, N., Kayan, İ., Vardar, S., Öner, E., Drahor, M., Göktürkler, G., Sengül, E., Erlat, E., Sütgibi, S., et al., Eds.; Environment, Society and Community from Prehistory to the Present; British Institute at Ankara: Ankara, Turkey, 2007; Volume 35, pp. 9–22.

43. Kayan, İ.; Vardar, S. Geomorphological formation and development of the delta plain of the Madra River. In *The Madra River Delta: Regional Studies on the Aegean Coast of Turkey 1*; Lambriandides, K., Spencer, N., Kayan, İ., Vardar, S., Öner, E., Drahor, M., Göktürkler, G., Sengül, E., Erlat, E., Sütgibi, S., et al., Eds.; Environment, Society and Community from Prehistory to the Present; British Institute at Ankara: Ankara, Turkey, 2007; Volume 35, pp. 23–30.

44. Kayan, İ.; Öner, E.; Kromer, B. Alluvial geomorphology and paleogeography of the Yeldeğirmeni mound and its environs. In *The Madra River Delta: Regional Studies on the Aegean Coast of Turkey 1*; Lambriandides, K., Spencer, N., Kayan, İ., Vardar, S., Öner, E., Drahor, M., Göktürkler, G., Sengül, E., Erlat, E., Sütgibi, S., et al., Eds.; Environment, Society and Community from Prehistory to the Present; British Institute at Ankara: Ankara, Turkey, 2007; Volume 35, pp. 31–38.

45. Wessel, B.; Huber, M.; Wohlfart, C.; Marschalk, U.; Kosmann, D.; Roth, A. Accuracy assessment of the global TanDEM-X Digital Elevation Model with GPS data. *ISPRS J. Photogramm. Remote. Sens.* **2018**, *139*, 171–182. [CrossRef]

46. Rizzoli, P.; Martone, M.; Gonzalez, C.; Wecklich, C.; Borla Tridon, D.; Bräutigam, B.; Bachmann, M.; Schulze, D.; Fritz, T.; Huber, M.; et al. Generation and performance assessment of the global TanDEM-X digital elevation model. *ISPRS J. Photogramm. Remote Sens.* **2017**, *132*, 119–139. [CrossRef]

47. OpenStreetMap Contributors. *OpenTopoMap*; QGIS QuickMapServices: 2020. Available online: https://plugins.qgis.org/plugins/quick_map_services/ (accessed on 21 September 2020).

48. Schneider, S.; Nykamp, M.; Matthaei, A.; Bebermeier, W.; Schütt, B. Alluvial geoarchaeology of a small drainage basin in western Anatolia: Late Holocene landscape development and the question of the mouth of the Paleo-Bakırçay. *Quat. Int.* **2013**, *312*, 84–95. [CrossRef]

49. Schneider, S.; Matthaei, A.; Bebermeier, W.; Schütt, B. Late Holocene human–environmental interactions in the Eastern Mediterranean: Settlement history and paleogeography of an ancient Aegean hill-top settlement. *Quat. Int.* **2014**, *324*, 84–98. [CrossRef]

50. Schneider, S.; Schlöffel, M.; Schwall, C.; Horejs, B.; Schütt, B. First stratigraphic evidence and absolute dating of a Bronze Age settlement in the Bakırçay valley in western Turkey. *J. Archaeol. Sci. Rep.* **2017**, *12*, 316–322. [CrossRef]

51. Schneider, S.; Matthaei, A.; Schlöffel, M.; Meyer, C.; Kronwald, M.; Pint, A.; Schütt, B. A geoarchaeological case study in the chora of Pergamon, western Turkey, to reconstruct the late Holocene landscape development and settlement history. *Quat. Int.* **2015**, *367*, 62–76. [CrossRef]

52. Crema, E.R.; Habu, J.; Kobayashi, K.; Madella, M. Summed Probability Distribution of 14C Dates Suggests Regional Divergences in the Population Dynamics of the Jomon Period in Eastern Japan. *PLoS ONE* **2016**, *11*, e0154809. [CrossRef] [PubMed]

53. Crema, E.; Bevan, A. Analysing Radiocarbon Dates Using the Rcarbon Package. 2020. Available online: https://cran.r-project.org/web/packages/rcarbon/vignettes/rcarbon.html (accessed on 28 April 2020).

54. Roberts, N.; Eastwood, W.J.; Kuzucuoğlu, C.; Fiorentino, G.; Caracuta, V. Climatic, vegetation and cultural change in the eastern Mediterranean during the mid-Holocene environmental transition. *Holocene* **2011**, *21*, 147–162. [CrossRef]

55. Fuchs, M. An assessment of human versus climatic impacts on Holocene soil erosion in NE Peloponnese, Greece. *Quat. Res.* **2007**, *67*, 349–356. [CrossRef]

56. Danacioğlu, Ş.; Tağil, Ş. Bakırçay Havzası'n RUSLE modeli kullanarak eroyzon riskinin değerlendirmesi. *Balıkesir Üniv. Sos. Bilim. Enst. Derg.* **2017**, *20*, 1–18.

57. Danacioğlu, Ş.; Tağil, Ş. Watershed management based on ecological risk characterization in Bakırçay watershed. *Fresenius Environ. Bull.* **2019**, *28*, 62–76.

58. Kottek, M.; Grieser, J.; Beck, C.; Rudolf, B.; Rubel, F. World Map of the Köppen-Geiger climate classification updated. *Meteorol. Z.* **2006**, 259–263. [CrossRef]

59. Rubel, F.; Brugger, K.; Haslinger, K.; Auer, I. The climate of the European Alps: Shift of very high resolution Köppen-Geiger climate zones 1800–2100. *Meteorol. Z.* **2017**, 115–125. [CrossRef]

60. Yang, X.; Becker, F.; Knitter, D.; Schütt, B. Geomorphological characterization of the Bakircay area. *Land* **2020**, submitted.

61. Yilmaz, Y.; Genç, Ş.C.; Gürer, F.; Bozcu, M.; Yilmaz, K.; Karacik, Z.; Altunkaynak, Ş.; Elmas, A. When Did the Western Anatolian Grabens Begin to Develop? *Geol. Soc. Lond. Spec. Publ.* **2000**, *173*, 353–384. [CrossRef]

62. Altunkaynak, Ş.; Yılmaz, Y. The Mount Kozak magmatic complex, Western Anatolia. *J. Volcanol. Geotherm. Res.* **1998**, *85*, 211–231. [CrossRef]

63. Harvey, A.M. Effective timescales of coupling within fluvial systems. *Geomorphology* **2002**, *44*, 175–201. doi:10.1016/S0169-555X(01)00174-X. [CrossRef]

64. Lewin, J.; Macklin, M.G.; Johnstone, E. Interpreting alluvial archives: Sedimentological factors in the British Holocene fluvial record. *Quat. Sci. Rev.* **2005**, *24*, 1873–1889. [CrossRef]

65. Hoffmann, T. Modelling the Holocene Sediment Budget of the Rhine System. Ph.D. Thesis, Mathematisch-Naturwissenschaftliche Fakult, Rheinische Friedrich-Willhelms-Universität Bonn, Bonn, Germany, 2006.

66. Richardson, J.M.; Fuller, I.C.; Macklin, M.G.; Jones, A.F.; Holt, K.A.; Litchfield, N.J.; Bebbington, M. Holocene river behaviour in New Zealand: Response to regional centennial-scale climate forcing. *Quat. Sci. Rev.* **2013**, *69*, 8–27. [CrossRef]

67. Macklin, M.G.; Jones, A.F.; Lewin, J. River response to rapid Holocene environmental change: Evidence and explanation in British catchments. *Quat. Sci. Rev.* **2010**, *29*, 1555–1576. [CrossRef]

68. R Core Team. *R: A Language and Environment for Statistical Computing*; R Foundation for Statistical Computing: Vienna, Austria, 2019. Available online: https://www.R-project.org/ (accessed on 21 September 2020).

69. Lemon, J. Plotrix: A package in the red light district of R. *R-News* **2006**, *6*, 8–12.

70. Bevan, A.; Crema, E.R. Rcarbon: Methods for Calibrating and Analysing Radiocarbon Dates. 2018. Available online: https://github.com/ahb108/rcarbon (accessed on 10 September 2020).

71. Neuwirth, E. RColorBrewer: ColorBrewer Palettes. 2014. Available online: https://CRAN.R-project.org/package=RColorBrewer (accessed on 18 May 2020).

72. Juggins, S. Rioja: Analysis of Quaternary Science Data. 2017. Available online: http://www.staff.ncl.ac.uk/stephen.juggins/ (accessed on 18 May 2020).

73. Wickham, H.; Averick, M.; Bryan, J.; Chang, W.; McGowan, L.D.; François, R.; Grolemund, G.; Hayes, A.; Henry, L.; Hester, J.; et al. Welcome to the tidyverse. *J. Open Source Softw.* **2019**, *4*, 1686. [CrossRef]

74. Zeileis, A.; Grothendieck, G. zoo: S3 Infrastructure for Regular and Irregular Time Series. *J. Stat. Softw.* **2005**, *14*, 1–27. [CrossRef]

75. QGIS Development Team. *QGIS Geographic Information System*; Open Source Geospatial Foundation: 2009. Available online: http://qgis.osgeo.org (accessed on 21 September 2020).

76. Inkscape Project. Inkscape Version 0.92.4 (2019-01-14). 2019. Available online: https://inkscape.org (accessed on 18 May 2020).

77. Reimer, P. IntCal13 and Marine13 Radiocarbon Age Calibration Curves 0–50,000 Years cal BP. *Radiocarbon* **2013**, *55*, 1869–1887. [CrossRef]

78. Weninger, B.; Clare, L.; Jöris, O.; Jung, R.; Edinborough, K. Quantum theory of radiocarbon calibration. *World Archaeol.* **2015**, *47*, 543–566. [CrossRef]

79. Walker, M.J.C.; Berkelhammer, M.; Björck, S.; Cwynar, L.C.; Fisher, D.A.; Long, A.J.; Lowe, J.J.; Newnham, R.M.; Rasmussen, S.O.; Weiss, H. Formal subdivision of the Holocene Series/Epoch: A Discussion Paper by a Working Group of INTIMATE (Integration of ice-core, marine and terrestrial records) and the Subcommission on Quaternary Stratigraphy (International Commission on Stratigraphy). *J. Quat. Sci.* **2012**, *27*, 649–659. [CrossRef]

80. Chiverrell, R.C.; Thorndycraft, V.R.; Hoffmann, T.O. Cumulative probability functions and their role in evaluating the chronology of geomorphological events during the Holocene. *J. Quat. Sci.* **2011**, *26*, 76–85. [CrossRef]

81. Jones, A.F.; Macklin, M.G.; Benito, G. Meta-analysis of Holocene fluvial sedimentary archives: A methodological primer. *CATENA* **2015**, *130*, 3–12. [CrossRef]

82. Lewin, J.; Macklin, M.G. Preservation potential for Late Quaternary river alluvium. *J. Quat. Sci.* **2003**, *18*, 107–120. [CrossRef]

83. Chiverrell, R.C.; Thorndycraft, V.R.; Hoffmann, T.O. Reply to comment: Cumulative probability functions and their role in evaluating the chronology of geomorphological events during the Holocene. Richard C. Chiverrell, Varyl, R. Thorndycraft and Thomas, O. Hoffmann, Journal of Quaternary Science 26: 76–85. *J. Quat. Sci.* **2011**, *26*, 241–244. [CrossRef]

84. Macklin, M.G.; Jones, A.F.; Lewin, J. Comment: Cumulative probability functions and their role in evaluating the chronology of geomorphological events during the Holocene. Richard C. Chiverrell, Varyl, R. Thorndycraft And Thomas, O. Hoffmann, Journal of Quaternary Science 26: 76–85. *J. Quat. Sci.* **2011**, *26*, 238–240. [CrossRef]

85. Carleton, W.C.; Groucutt, H. Sum things are not what they seem: Problems with the interpretation and analysis of radiocarbon-date proxies. *SocArXiv* **2019**. [CrossRef]

86. Hoffmann, T.; Lang, A.; Dikau, R. Holocene river activity: Analysing 14C-dated fluvial and colluvial sediments from Germany. *Quat. Sci. Rev.* **2008**, *27*, 2031–2040. [CrossRef]

87. Macklin, M.G.; Johnstone, E.; Lewin, J. Pervasive and long-term forcing of Holocene river instability and flooding in Great Britain by centennial-scale climate change. *Holocene* **2005**, *15*, 937–943. [CrossRef]

88. Williams, A.N. The use of summed radiocarbon probability distributions in archaeology: A review of methods. *J. Archaeol. Sci.* **2012**, *39*, 578–589. [CrossRef]

89. Sadler, P.M. Sediment Accumulation Rates and the Completeness of Stratigraphic Sections. *J. Geol.* **1981**, *89*, 569–584. [CrossRef]

90. Schumer, R.; Jerolmack, D.J. Real and apparent changes in sediment deposition rates through time. *J. Geophys. Res. Earth Surf.* **2009**, *114*. [CrossRef]

91. Surovell, T.A.; Byrd Finley, J.; Smith, G.M.; Brantingham, P.J.; Kelly, R. Correcting temporal frequency distributions for taphonomic bias. *J. Archaeol. Sci.* **2009**, *36*, 1715–1724. [CrossRef]

92. Rhode, D.; Brantingham, P.J.; Perreault, C.; Madsen, D.B. Mind the gaps: Testing for hiatuses in regional radiocarbon date sequences. *J. Archaeol. Sci.* **2014**, *52*, 567–577. [CrossRef]

93. Orton, D.; Morris, J.; Pipe, A. Catch Per Unit Research Effort: Sampling Intensity, Chronological Uncertainty, and the Onset of Marine Fish Consumption in Historic London. *Open Quat.* **2017**, *3*, 1–20. [CrossRef]

94. Contreras, D.A.; Meadows, J. Summed radiocarbon calibrations as a population proxy: A critical evaluation using a realistic simulation approach. *J. Archaeol. Sci.* **2014**, *52*, 591–608. [CrossRef]

95. Brown, W.A. Through a filter, darkly: Population size estimation, systematic error, and random error in radiocarbon-supported demographic temporal frequency analysis. *J. Archaeol. Sci.* **2015**, *53*, 133–147. [CrossRef]

96. Shennan, S.; Downey, S.S.; Timpson, A.; Edinborough, K.; Colledge, S.; Kerig, T.; Manning, K.; Thomas, M.G. Regional population collapse followed initial agriculture booms in mid-Holocene Europe. *Nat. Commun.* **2013**, *4*, 1–8. [CrossRef]

97. Timpson, A.; Colledge, S.; Crema, E.; Edinborough, K.; Kerig, T.; Manning, K.; Thomas, M.G.; Shennan, S. Reconstructing regional population fluctuations in the European Neolithic using radiocarbon dates: A new case-study using an improved method. *J. Archaeol. Sci.* **2014**, *52*, 549–557. [CrossRef]

98. van der Plicht, J. Radiocarbon, the Calibration Curve and Scythian Chronology. In *Impact of the Environment on Human Migration in Eurasia*; Marian Scott, E., Alekseev, A.Y., Zaitseva, G., Eds.; Kluwer Academic: Dordrecht, The Netherlands, 2004; pp. 45–61.

99. Finné, M.; Woodbridge, J.; Labuhn, I.; Roberts, C.N. Holocene hydro-climatic variability in the Mediterranean: A synthetic multi-proxy reconstruction. *Holocene* **2019**. [CrossRef]

100. Roberts, N.; Jones, M.; Benkaddour, A.; Eastwood, W.; Filippi, M.; Frogley, M.; Lamb, H.; Leng, M.; Reed, J.; Stein, M.; et al. Stable isotope records of Late Quaternary climate and hydrology from Mediterranean lakes: The ISOMED synthesis. *Quat. Sci. Rev.* **2008**, *27*, 2426–2441. [CrossRef]

101. Dormoy, I.; Peyron, O.; Combourieu Nebout, N.; Goring, S.; Kotthoff, U.; Magny, M.; Pross, J. Terrestrial climate variability and seasonality changes in the Mediterranean region between 15 000 and 4000 years BP deduced from marine pollen records. *Clim. Past* **2009**, *5*, 615–632. [CrossRef]

102. Connor, S.E.; Ross, S.A.; Sobotkova, A.; Herries, A.I.; Mooney, S.D.; Longford, C.; Iliev, I. Environmental conditions in the SE Balkans since the Last Glacial Maximum and their influence on the spread of agriculture into Europe. *Quat. Sci. Rev.* **2013**, *68*, 200–215. [CrossRef]

103. Foley, S.F.; Gronenborn, D.; Andreae, M.O.; Kadereit, J.W.; Esper, J.; Scholz, D.; Pöschl, U.; Jacob, D.E.; Schöne, B.R.; Schreg, R.; et al. The Palaeoanthropocene–The beginnings of anthropogenic environmental change. *Anthropocene* **2013**, *3*, 83–88. [CrossRef]

104. Roberts, C.N.; Woodbridge, J.; Palmisano, A.; Bevan, A.; Fyfe, R.; Shennan, S. Mediterranean landscape change during the Holocene: Synthesis, comparison and regional trends in population, land cover and climate. *Holocene* **2019**, *29*, 923–937. [CrossRef]

105. Weiberg, E.; Bevan, A.; Kouli, K.; Katsianis, M.; Woodbridge, J.; Bonnier, A.; Engel, M.; Finné, M.; Fyfe, R.; Maniatis, Y.; et al. Long-term trends of land use and demography in Greece: A comparative study. *Holocene* **2019**, *29*, 742–760. [CrossRef]

106. Woodbridge, J.; Roberts, C.N.; Palmisano, A.; Bevan, A.; Shennan, S.; Fyfe, R.; Eastwood, W.J.; Izdebski, A.; Çakırlar, C.; Woldring, H.; et al. Pollen-inferred regional vegetation patterns and demographic change in Southern Anatolia through the Holocene. *Holocene* **2019**, *29*, 728–741. [CrossRef]

107. Eastwood, W.J.; Roberts, N.; Lamb, H.F. Palaeoecological and Archaeological Evidence for Human Occupance in Southwest Turkey: The Beyşehir Occupation Phase. *Anatol. Stud.* **1998**, *48*, 69–86. [CrossRef]

108. Çilingiroglu, C. *Central-West Anatolia at the end of 7th and Beginning of 6th Millennium BCE in the Light of Pottery from Ulucak (Izmir)*; Universität Tübingen: Tübingen, Germany, 2009.

109. Düring, B.S. *The Prehistory of Asia Minor: From Complex Hunter-Gatheres to Early Urban Societies*; Cambridge University Press: Cambridge, UK, 2010.

110. Horejs, B.; Milić, B.; Pavúk, P. Der prähistorische Umlandsurvey. In *Pergamon—Bericht über die Arbeiten in der Kampagne 2014*; Pirson, F., Ed.; Archäologischer Anzeiger; Deutsches Archäologisches Institut/German Archaeological Institute: Berlin, Germany, 2015; Volume 2, pp. 134–139.

111. Horejs, B.; Schwall, C. Der prähistorische Umlandsurvey. In *Pergamon—Bericht über die Arbeiten in der Kampagne 2015*; Pirson, F., Ed.; Archäologischer Anzeiger; Deutsches Archäologisches Institut/German Archaeological Institute: Berlin, Germany, 2016; Volume 2, pp. 170–172.

112. Horejs, B. Der prähistorische Umlandsurvey. In *Pergamon—Bericht über die Arbeiten in der Kampagne 2012*; Pirson, F., Ed.; Archäologischer Anzeiger; Deutsches Archäologisches Institut/German Archaeological Institute: Berlin, Germany, 2013; Volume 2, pp. 109–118.

113. Berger, J.F.; Lespez, L.; Kuzucuoğlu, C.; Glais, A.; Hourani, F.; Barra, A.; Guilaine, J. Interactions between climate change and human activities during the early to mid-Holocene in the eastern Mediterranean basins. *Clim. Past* **2016**, *12*, 1847–1877. [CrossRef]

114. Dreibrodt, S.; Lubos, C.; Lomax, J.; Sipos, G.; Schroedter, T.; Nelle, O. Holocene landscape dynamics at the tell Arslantepe, Malatya, Turkey—Soil erosion, buried soils and settlement layers, slope and river activity in a middle Euphrates catchment. *Holocene* **2014**, *24*, 1351–1368. [CrossRef]

115. Weiss, H. Global megadrought, societal collapse and resilience at 4.2-3.9 ka BP across the Mediterranean and west Asia. *PAGES Mag.* **2016**, *24*, 62–63. [CrossRef]

116. Bini, M.; Zanchetta, G.; Perşoiu, A.; Cartier, R.; Català, A.; Cacho, I.; Dean, J.R.; Rita, F.D.; Drysdale, R.N.; Finnè, M.; et al. The 4.2 ka BP Event in the Mediterranean region: An overview. *Clim. Past* **2019**, *15*, 555–577. [CrossRef]

117. Gasse, F. Hydrological changes in the African tropics since the Last Glacial Maximum. *Quat. Sci. Rev.* **2000**, *19*, 189–211. [CrossRef]

118. Gasse, F. Continental palaeohydrology and palaeoclimate during the Holocene. *C. R. Geosci.* **2005**, *337*, 79–86. [CrossRef]

119. Devillers, B. Morphogenèse et Anthropisation Holocènes d'un Bassin Versant Semi-Aride: Le Gialias, Chypre. Ph.D. Dissertation, Université de Provence-Aix-Marseille I, Aix-en-Provence, France, 2005.

120. Rita, F.D.; Molisso, F.; Sacchi, M. Late Holocene environmental dynamics, vegetation history, human impact, and climate change in the ancient Literna Palus (Lago Patria; Campania, Italy). *Rev. Palaeobot. Palynol.* **2018**, *258*, 48–61. [CrossRef]

121. Isola, I.; Zanchetta, G.; Drysdale, R.N.; Regattieri, E.; Bini, M.; Bajo, P.; Hellstrom, J.C.; Baneschi, I.; Lionello, P.; Woodhead, J.; et al. The 4.2 ka event in the central Mediterranean: New data from a Corchia speleothem (Apuan Alps, central Italy). *Clim. Past* **2019**, *15*, 135–151. [CrossRef]

122. Allcock, S.L.; Roberts, N. Changes in regional settlement patterns in Cappadocia (central Turkey) since the Neolithic: A combined site survey perspective. *Anatol. Stud.* **2014**, *64*, 33–57. [CrossRef]

123. Weiss, H. 4.2 ka BP Megadrought and the Akkadian Collapse. In *Megadrought and Collapse: From Early Agriculture to Angkor*; Oxford University Press: Oxford, UK, 2017.

124. Ghilardi, M.; Cordier, S.; Carozza, J.M.; Psomiadis, D.; Guilaine, J.; Zomeni, Z.; Demory, F.; Delanghe-Sabatier, D.; Vella, M.A.; Bony, G.; et al. The Holocene fluvial history of the Tremithos river (south central Cyprus) and its linkage to archaeological records. *Environ. Archaeol.* **2015**, *20*, 184–201. [CrossRef]

125. Francke, A.; Wagner, B.; Leng, M.J.; Rethemeyer, J. A Late Glacial to Holocene record of environmental change from Lake Dojran (Macedonia, Greece). *Clim. Past* **2013**, *9*, 481–498. [CrossRef]

126. Bakker, J.; Kaniewski, D.; Verstraeten, G.; De Laet, V.; Waelkens, M. Numerically derived evidence for late-Holocene climate change and its impact on human presence in the southwest Taurus Mountains, Turkey. *Holocene* **2012**, *22*, 425–438. [CrossRef]

127. Vermoere, M.; Smets, E.; Waelkens, M.; Vanhaverbeke, H.; Librecht, I.; Paulissen, E.; Vanhecke, L. Late Holocene Environmental Change and the Record of Human Impact at Gravgaz near Sagalassos, Southwest Turkey. *J. Archaeol. Sci.* **2000**, *27*, 571–595. [CrossRef]

128. PIrson, F. Die Siedlungsgeschichte Pergamons–Überblick und kritische Revision Mit einem Appendix von Anneke Keweloh-Kaletta. *Istanbuler Mitteilungen* **2017**, *67*, 43–103.

129. Wulff, U. Der Stadtplan von Pergamon. Zur Entwicklung und Stadtstruktur von der Neugriindung unter Philetairos bis in spatantike Zeit. *Istanbuler Mitteilungen* **1994**, *44*, 135–175.

130. Kobes, J. Fremdes Getreide. Beobachtungen zum Problem der Getreideversorgung in der kaiserzeitlichen Provinz Asia. *Laverna* **1999**, *10*, 81–98.

131. Sommerey, K.M. Die Chora von Pergamon–Studien zu Grenzen, Siedlungsstruktur und Wirtschaft. *Istanbuler Mitteilungen* **2008**, *58*, 135–170.

132. Borrelli, P.; Domdey, C.; Hoelzmann, P.; Knitter, D.; Panagos, P.; Schütt, B. Geoarchaeological and historical implications of late Holocene landscape development in the Carseolani Mountains, central Apennines, Italy. *Geomorphology* **2014**, *216*, 26–39. [CrossRef]

133. Rosen, A.M. Environmental Change and Settlement at Tel Lachish, Israel. *Bull. Am. Sch. Orient. Res.* **1986**, *263*, 55–60. [CrossRef]

134. Dotterweich, M. The history of human-induced soil erosion: Geomorphic legacies, early descriptions and research, and the development of soil conservation—A global synopsis. *Geomorphology* **2013**, *201*, 1–34. [CrossRef]

135. Haenssler, E.; Nadeau, M.J.; Vött, A.; Unkel, I. Natural and human induced environmental changes preserved in a Holocene sediment sequence from the Etoliko Lagoon, Greece: New evidence from geochemical proxies. *Quat. Int.* **2013**, *308–309*, 89–104. [CrossRef]

136. Roberts, N.; Allcock, S.L.; Barnett, H.; Mather, A.; Eastwood, W.J.; Jones, M.; Primmer, N.; Yiğitbaşıoğlu, H.; Vannière, B. Cause-and-effect in Mediterranean erosion: The role of humans and climate upon Holocene sediment flux into a central Anatolian lake catchment. *Geomorphology* **2019**, *331*, 36–48. [CrossRef]

137. Walsh, K.; Berger, J.F.; Roberts, C.N.; Vanniere, B.; Ghilardi, M.; Brown, A.G.; Woodbridge, J.; Lespez, L.; Estrany, J.; Glais, A.; et al. Holocene demographic fluctuations, climate and erosion in the Mediterranean: A meta data-analysis. *Holocene* **2019**. [CrossRef]

138. Bakker, J.; Paulissen, E.; Kaniewski, D.; De Laet, V.; Verstraeten, G.; Waelkens, M. Man, vegetation and climate during the Holocene in the territory of Sagalassos, Western Taurus Mountains, SW Turkey. *Veg. Hist. Archaeobotany* **2012**, *21*, 249–266. [CrossRef]

139. Vanmaercke, M.; Poesen, J.; Govers, G.; Verstraeten, G. Quantifying human impacts on catchment sediment yield: A continental approach. *Glob. Planet. Chang.* **2015**, *130*, 22–36. [CrossRef]

140. Dotterweich, M. The history of soil erosion and fluvial deposits in small catchments of central Europe: Deciphering the long-term interaction between humans and the environment—A review. *Geomorphology* **2008**, *101*, 192–208. [CrossRef]

141. Vandam, R.; Kaptijn, E.; Broothaerts, N.; Cupere, B.D.; Marinova, E.; Loo, M.V.; Verstraeten, G.; Poblome, J. "Marginal" Landscapes: Human Activity, Vulnerability, and Resilience in the Western Taurus Mountains (Southwest Turkey). *J. East. Mediterr. Archaeol. Herit. Stud.* **2019**, *7*, 432–450. [CrossRef]

142. Ludwig, B.; Knitter, D. Pergamon und seine Mikroregion–Räumliche Analysen zur Siedlungsstrukturin der Römischen Kaiserzeit (1. Jh. v. Chr.—4. Jh. n. Chr.). Presented at the 13th Internationales Kolloquium zur Historischen Geographie des Altertums, Eichstätt, Germany, 5–8 July 2017, unpublished.

143. Notebaert, B.; Verstraeten, G. Sensitivity of West and Central European river systems to environmental changes during the Holocene: A review. *Earth-Sci. Rev.* **2010**, *103*, 163–182. [CrossRef]

144. Pavúk, P.; Horejs, B. Ceramics, Surveys, and Connectivity in Western Anatolia: The Middle and Late Bronze Age Bakırçay/Kaikos Valley Restudied. *Egypt Levant. Int. J. Egypt. Archaeol. Relat. Discip.* **2018**, *28*, 457–486. [CrossRef]